Missing sea-level rise in southeast Greenland during and since the Little Ice Age

Sarah A. Woodroffe[1], Leanne M. Wake[2], Kristian K. Kjeldsen[3], Natasha L.M. Barlow[4], Antony J. Long[1], Kurt H. Kjær[5]

[1]Department of Geography, Durham University, Lower Mountjoy, South Road, Durham, DH1 3LE, UK, s.a.woodroffe@durham.ac.uk

[2]Department of Geography and Environmental Sciences, Northumbria University, Ellison Place, Newcastle upon Tyne, NE1 8ST, UK, leanne.wake@northumbria.ac.uk

[3]Geological Survey of Denmark and Greenland (GEUS), 1350 Copenhagen K, Denmark, kkk@geus.dk

[4]School of Earth and Environment, University of Leeds, LS2 9JT, UK, n.l.m.barlow@leeds.ac.uk

[5]GeoGenetics, Globe Institute, University of Copenhagen, 1350 Copenhagen K, Denmark, kurtk@sund.ku.dk

Correspondence to: Sarah A. Woodroffe (s.a.woodroffe@durham.ac.uk)

Abstract

The Greenland Ice Sheet has been losing mass at an accelerating rate over the past two decades. Understanding ice mass and glacier changes during the preceding several hundred years, prior to geodetic measurements, is more difficult because evidence of past ice extent in many places was later overridden. Saltmarshes provide the only continuous records of Relative Sea Level (RSL) from close to the Greenland Ice Sheet that span the period of time during and since the Little Ice Age (LIA) and can be used to reconstruct ice mass gain and loss over recent centuries. Saltmarsh sediments collected at the mouth of Dronning Marie Dal, close to the Greenland Ice Sheet margin in southeast Greenland, record RSL changes over the past c. 300 years through changing sediment and diatom stratigraphy. These RSL changes record a combination of processes that are dominated by local/regional changes in

Greenland Ice Sheet mass balance during this critical period that spans the maximum of the LIA and 20th Century warming. In the early part of the record (1725-1762 CE) the rate of RSL rise is higher than reconstructed from the closest isolation basin at Timmiarmiut, but between 1762-1880 CE the RSL rate is within the error range of rate of RSL change recorded in the isolation basin. RSL begins to slowly fall around 1880 CE and then accelerates since the 1990s, with a total amount of RSL fall of 0.09~~8~~ ±0.1 m in the last 140 years. Modelled RSL, which takes into account contributions from post-LIA Greenland Ice Sheet Glacio-isostatic Adjustment (GIA), ongoing deglacial GIA, the global non-ice sheet glacial melt fingerprint, contributions from thermosteric effects, the Antarctic mass loss sea-level fingerprint and terrestrial water storage, over-predicts the amount of RSL fall since the end of the LIA by at least 0.5 m. The GIA signal caused by post-LIA Greenland Ice Sheet mass loss is by far the largest contributor to this modelled RSL, and error in its calculation has ~~canmay have~~ a large impact on RSL predictions at Dronning Marie Dal. We cannot reconcile the modelled RSL and the saltmarsh observations, even when moving the termination of the LIA to 17~~8~~00 CE and reducing the post-LIA Greenland mass loss signal by 30 %, and a 'budget residual' of +~2.5~~3~~ mm/yr since the end of the LIA remains unexplained. This new RSL record backs up other studies which suggest that there are significant regional differences in the timing and magnitude of the response of the Greenland Ice Sheet to the climate shift from the LIA into the 20th Century.

Keywords: Greenland, relative sea level, saltmarsh, glacio-isostatic adjustment, Little Ice Age, sea-level budget

1.   Introduction

Studies using a range of different geodetic methods all agree that the Greenland Ice Sheet ~~ice sheet~~ (GrIS) has been losing mass at an accelerating rate over the past two decades (Bevis et al., 2019, 2012; Chen et al., 2021; Khan et al., 2015; Moon et al., 2012; Pritchard et al., 2009; The IMBIE Team, 2020; van den Broeke et al., 2009). There is however less known about when and at what rate ice mass loss occurred in Greenland during the last millennium until the start of the satellite and GPS eras, when Greenland underwent ~~during~~ periods of climate warming and cooling (Briner et al., 2020; Khan et al., 2020; Kjær et al., 2022). Using Little Ice Age (LIA) trimlines and stereo-photogrammetric imagery

recorded between 1978-1987, Kjeldsen et al. (2015) estimated an average Greenland-wide total ice mass loss of c. 75 Gt/yr during the 20th Century. However, understanding how the rate of mass loss varied during the 20th Century is more complex because it requires us to put a date on the end of the LIA, and to find a way of reconstructing mass loss fluctuations without the help of continuous geodetic data. Understanding ice mass and glacier changes during the preceding several hundred years is even more difficult because evidence of past ice sheet extent in many places has been overridden by later advances (Briner et al., 2011; Kjær et al., 2022).

Salt marshes in nearfield settings record the timing and magnitude of fluctuations in ice mass during the last few centuries through changes in relative sea-level (RSL) (e.g. Long et al., 2012). RSL reflects the interplay of different cryosphere and oceanic processes but the dominant process close to an ice sheet is the visco-elastic signature of local and regional mass changes through time (Farrell and Clark, 1976). Salt marshes form in the upper part of the intertidal zone and can continuously accumulate organic sediment (Allen, 2000). Salt marshes in Greenland are generally small features with a very short growing season, low sedimentation rates and may be affected by interactions with winter shore-fast ice (Lepping and Daniëls, 2007). However, they can survive in these conditions and provide the only continuous records of RSL from close to the GrIS that span the period during and since the LIA and can be used to reconstruct ice mass gain and loss over recent centuries (Long et al., 2012, 2010; Woodroffe and Long, 2009).

This study reports for the first time a continuous RSL record over the past ~300 years from a salt marsh within 5 km of the ice sheet margin in southeast Greenland. The sediments and plant remains in the marsh record RSL fluctuations over the last few hundred years and therefore provide a unique record of changes in regional RSL during and since the LIA in Greenland. We predict local RSL changes by creating a sea-level budget which includes predictions from a Glacio-Isostatic Adjustment (GIA) model with c. 430 Gt ice mass loss in southeast Greenland between the end of the LIA and 2010 (as defined by Kjeldsen et al., 2015), and estimates of other contributions since the end of the LIA including mass loss from Greenland peripheral glaciers, non-Greenland ice, the thermosteric contribution and the effect of terrestrial water storage in the 20th and 21st Centuries. Comparing the modelled sea-level budget and

3

86   the saltmarsh data provides an opportunity to consider potential errors in both methods and suggest how

87   we might bring model and data estimates closer together, as well as develop better understanding of the

88   nature of historical RSL in southeast Greenland and implications for coastline response to future,

89   enhanced GrIS and peripheral glacier melt.

90

91   **2. Study site and methods**

92   *2.1 Field site and glacial history of the region*

93   The saltmarsh record is from 63.470°N, -41.925°W at the head of Dronning Marie Dal in southeast

94   Greenland (Figure 1A,B, Fig 2). The saltmarsh is fed by freshwater and sediment from Dronning Marie

95   Dal, a formerly glaciated valley that drains part of the nearby Skinfaxe outlet glacier. Dronning Marie

96   Dal is at the head of the 50 km long marine fjord Søndre Skjoldungesund which together with Nørre

97   Skjoldungesund encompass the glaciated island of Skjoldungen (Figure 1C). The northern fjord has a

98   bedrock sill mid-fjord at c. 215 m below sea level, while the southern fjord has a narrow central section

99   with a sill located at 77 m below sea level (Kjeldsen et al., 2017). The narrow stretch connecting the

100   two fjords at their inland extent is generally shallow, sheltering the salt marsh at Dronning Marie Dal.

101   The region is dominated by long, steep-sided marine fjords with the GrIS ending at the coast in marine-

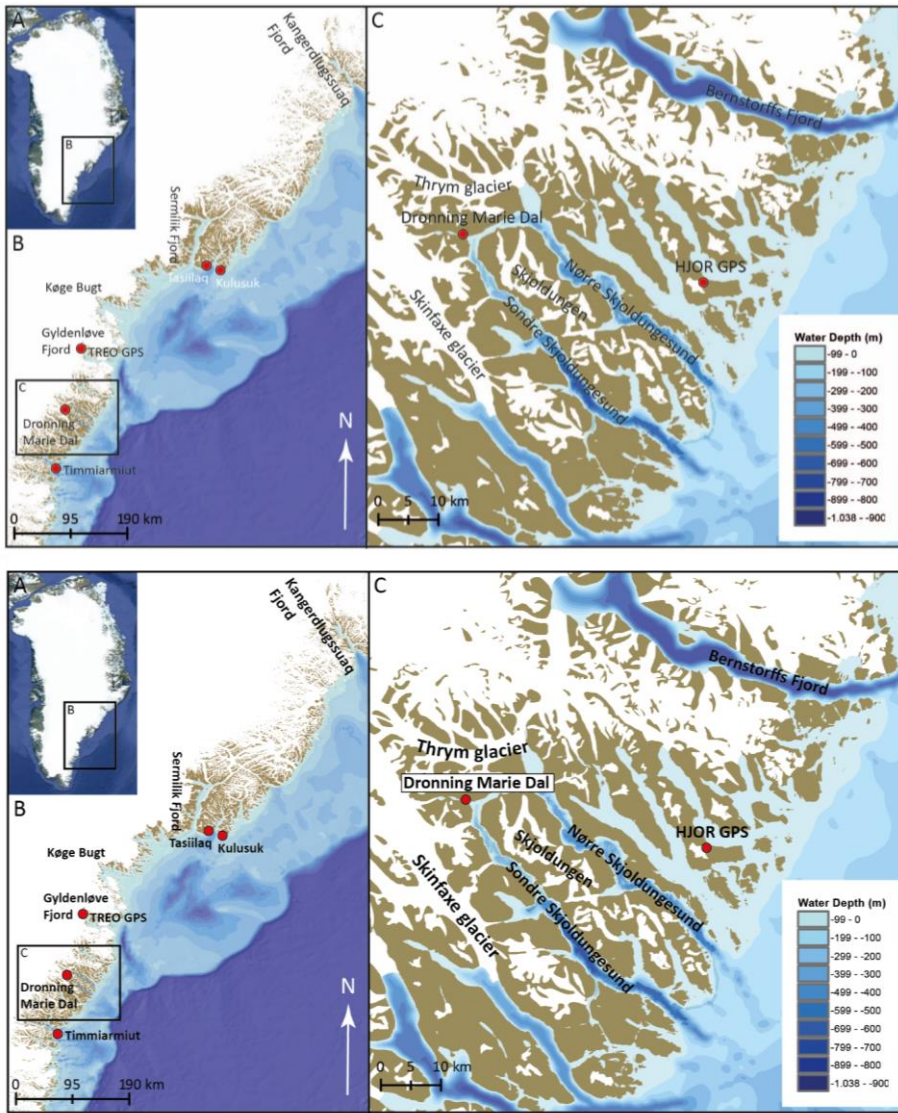102   terminating outlet glaciers.

4

Figure 1. A) Map of Greenland © Google Earth, B) Southeast Greenland region showing the location of the field site (Dronning Marie Dal) alongside other studied fjords, C) Dronning Marie Dal saltmarsh at the head of Sondre Skjoldungesund, between the Skinfaxe and Thrum glacier margins.

108 Relatively little is known about the deglacial history of the southeast compared to the southwest of

109 Greenland. Most work has been undertaken in the large fjords (e.g. Kangerdlugssuaq, Sermilik, Køge

110 Bugt, Gyldenløve, Bernstorffs Fjord, Figure 1) to the north of the field area using [10]Be measurements

111 to reconstruct fjord deglaciation. During the LGM the ice sheet reached the shelf edge (50-80 km from

112 the outer coast) in this region and in the offshore Kangerdlugssuaq Trough to the north of the study area

113 the ice sheet started to retreat by c. 17 ka BP (Funder et al., 2011). Onshore deglaciation at the outer

114 coast occurred earlier to the north (Kangerdlugssuaq - 11.8 +/- 1ka BP) compared to the south

115 (Bernstorffs Fjord - 10.4 +/- 450 ka BP), driven by incursion of warm Atlantic water into the fjords

116 from the Irminger Current, moderated by local coastal bathymetry and atmospheric warming during the

117 early Holocene (Dyke et al., 2018, 2014; Hughes et al., 2012). [10]Be dates on boulders from outer and

118 inner Skjoldungesund suggest deglaciation here occurred in the early Holocene (inner fjord by 10.4

119 ±0.4 ka BP) (Levy et al., 2020). Following retreat from the shelf edge, the deglaciation model HUY3

120 simulates retreat onshore by 10 ka BP, which largely agrees with the field evidence from

121 Skjoldungesund, with the ice sheet slightly inland of its LIA maximum position at 4 ka BP (Lecavalier

122 et al., 2014). The deglacial marine limit is low in this region (c. 20-40 m) suggesting less deglacial

123 mass loss compared to elsewhere in Greenland (Funder and Hansen, 1996). Observations of strandlines

124 up to 75 m above sea level in this region, reported by Vogt (1933) are cut into bedrock and are highly

125 unlikely to be of marine origin.

126

127 The HUY3 geophysical model predicts slight crustal subsidence at the coast today caused primarily by

128 a local late Holocene neoglacial readvance (resulting in RSL rise of 1-1.5 mm/yr over the last 1000

129 years) (Lecavalier et al., 2014). However, a recent GPS-derived GIA model (GNET-GIA) offers an

130 alternative solution with GIA uplift calculated at +2.8mm/yr and +3.1 mm/yr at nearby HJOR and

131 TREO GPS sites (Figure 1), which would result in pre-20th Century RSL fall at Dronning Marie Dal

132 (Khan et al., 2016). By comparing GPS data and absolute gravity observations over a 20-year period,

133 van Dam et al (2017) also suggest ongoing GIA uplift of +4.5 +/- 1.4 mm/yr at Kulusuk (300 km to the

134 north). These GIA estimates, based on modern observations, are corrected for elastic deformation in

135 response to modern mass balance changes to predict ongoing deglacial GIA. The most recent

136 examination of Greenland GIA model outputs and GPS data by Adhikari et al. (2021) suggests that

residual uplift caused by mass loss since the Medieval Warm Period, and in particular since the LIA, accompanied by a reduced mantle viscosity on sub-centennial timescales, can explain the observed discrepancy between uplift rates from HUY3 and elastic-corrected GPS uplift rates around Greenland.

LIA moraines are situated ~~beyond~~ ahead of~~n~~ the current frontal margins of ~~the GrIS and local glaciers in this region and demonstrate clearly that glacial retreat has occurred during the 20th Century (Bjork et al., 2012). The instrumental temperature record from Tasiilaq indicates 2°C per decade of warming between 1919 and 1932 CE (the early twentieth-century warming (ECW)), followed by cooling during the 1950's to 1970's and steady temperature rise of 1.3°C per decade since 1993 (Bjork et al., 2012; Chylek et al., 2006; Wood and Overland, 2010). Despite these decadal temperature fluctuations, and the overall pattern of post-LIA retreat of southeast Greenland glaciers, the nearest glaciers to the field site (Skinfaxe and Thrym, Figure 1C) have been relatively stable at their present positions since at least the 1930s (Bjork et al., 2012). It is important to note however that Skinfaxe sits on a ledge in its fjord system so would require significant thinning to dislodge it from its current position and Thrym Glacier appears to be resting on a shallow ~~prograding~~ bedrock rise (Bjork et al., 2012; Morlighem et al., 2017). The total ice mass loss from the two drainage basins closest to the field site (Central East and South-East in Kjeldsen et al., 2015) is 249 Gt between the end of the LIA and 1983, 134 Gt between 1983 and 2003 and 45 Gt between 2003 and 2010, based on the volume of loss from LIA trimlines and more recent air photos. There is a significant increase (~70%) in the amount of regional mass loss during the post-1983 period compared to earlier in the 20th Century. We hypothesise that regional ice mass loss since the end of the LIA should produce a visco-elastic GIA response recorded as variable 20th century RSL change by local salt marsh sediments, such as those at Dronning Marie Dal (Figure 2).

Commented [le1]: When I read this, I interpreted as 'behind' . So I've changed to 'ahead of'
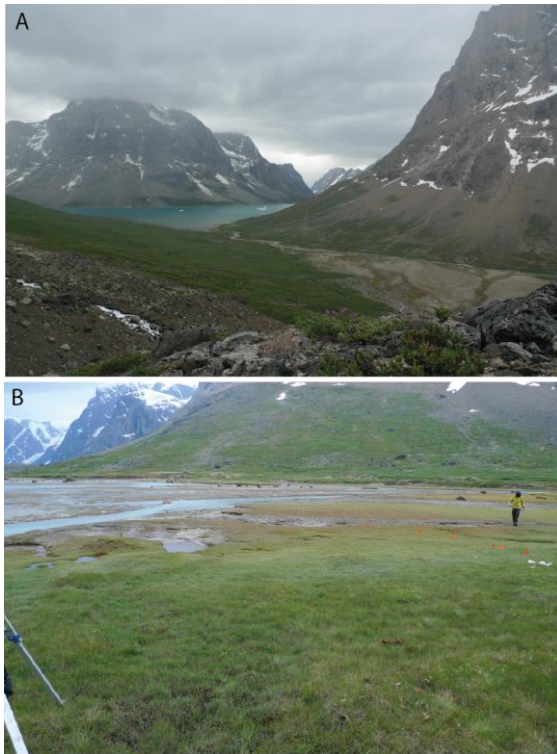
Figure 2. A) photograph looking East down the Dronning Marie Dal valley towards the head of Sondre Skoldungesund and the salt marsh where the valley meets the fjord. B) photograph of the Dronning Marie Dal salt marsh showing the low-angled relief of the marsh and zonation of salt marsh vegetation (high marsh in the foreground).

2.2 Reconstructing RSL using saltmarsh sediments

We collected salt marsh sediments by digging a small pit using a spade from the present-day high salt marsh at the mouth of Dronning Marie Dal (Figure 1C, 2). The analysed sediment section is 13 cm thick, with organic silt containing saltwater-tolerant diatoms situated over compacted sand-rich silt where no diatoms are present (Figure 3). We sampled the fossil sediment section at 0.25 cm intervals in the top 1 cm, and at 0.5 cm intervals further downcore to provide high-resolution RSL estimates, bearing in mind the slow rate of sedimentation in most Greenlandic salt marshes (Long et al., 2012; Woodroffe and Long, 2009). To reconstruct local RSL we investigated diatom assemblages across the

8

present-day salt marsh in the same location to understand changes in assemblages with elevation across the upper part of the intertidal zone (Figure 3A). We then compared these assemblages to those found through the sediment core using a visual assessment technique, that places weight on certain ~~key~~ taxa that change abundance at clearly defined elevations (Long et al., 2012, 2010; Woodroffe and Long, 2009). The main species used to reconstruct RSL are the high marsh/freshwater species *Pinnularia intermedia*, ~~and~~ and the high to low marsh species *Navicula cincta* and *Navicula salinarum*. Using elevation zones inhabited by key species alone to reconstruct RSL introduces artificial jumps into a RSL record when moving from a sample reconstructed from within one zone to the next sample which may be reconstructed in a different zone. To create an RSL reconstruction with no artificial jumps within it we use a smoothing function which allows the PMSE (palaeo-marsh surface elevation) to change within each zone, noting the progressive way that the key diatom taxa change up core. For instance the progressive rise in *Pinnularia intermedia* in the top 4 cm suggests smoothly falling RSL during this period. We therefore modify the ~~palaeo-marsh surface elevation~~ PMSE results for the zoned reconstruction to allow for the progressive change seen in the diatoms (Table S2). This is backed up by the LOI data which suggests a progressive rise in organic content in the top 4 cm indicative of rising PMSE. We prefer this method over a transfer function approach (e.g. Barlow et al., 2013) because it relies on certain indicator species that occur at narrowly defined levels, but also utilises other evidence such as vertical diatom succession and the stratigraphy to interpret changes in RSL. In addition we do not tune the RSL reconstructions to present day RSL, rather the most recent index point reflects its diatom-based reconstruction and therefore present day RSL lies within the vertical error term of this reconstruction. This is done to prevent a spurious jump in recent RSL caused by a vertical offset between the mid-point in the earlier diatom-based reconstructions and the present-day marsh-surface elevation, which would happen if this was used to tune the core-top sample reconstruction.

We initially calculated the elevations of modern and fossil saltmarsh samples to mean sea level (MSL) using a high-precision dGPS. However due to technical issues with post-processing we instead rely on tidal data from Timmiarmiut (100 km to the S) and tidal predictions from Tasiilaq (300 km to the NE) collected during our fieldwork, along with knowledge about saltmarsh vegetation zonation in Greenland and their general relationship to tidal levels, to relate fossil and modern saltmarsh elevations to mean

9

218 sea level (MSL). The tidal data from Timmiarmiut show that although the timing of daily tidal

219 fluctuations differs to predictions for Tasiilaq, the amplitude of tidal fluctuations is remarkably similar

220 (within 0.1 m). The tidal range (lowest to highest astronomical tide) at the outer coast is approximately

221 3.7 m. We have some confidence therefore that tidal predictions for Tasiilaq are applicable (with a time

222 correction) along the outer coast anywhere between Tasiilaq and Timmiarmiut, although the distances

223 involved are large. This leaves the issue of tidal range amplification or dampening in fjord-head settings

224 to consider, as the Dronning Marie Dal site is c. 50 km up-fjord from the open ocean (Figure 1C). This

225 is considered elsewhere in Greenland by Richter et al., (2011) who show that this effect is variable due

226 to fjord bathymetry and cross-section geometry, and ranges from -9 cm to +14 cm up fjord compared

227 to the fjord mouths on the west coast in fjords of similar length to Søndre Skoldungesund. Modern

228 saltmarsh vegetation at Dronning Marie Dal grows between 0.1 m above Highest Astronomical Tide

229 (HAT) and 0.08 m below Mean High Water of Spring Tide (MHWST) levels, which is very similar to

230 saltmarsh vegetation ranges we have observed elsewhere in southeast and southwest Greenland

231 (unpublished data and Woodroffe and Long, 2010, 2009). We are therefore confident that any effect of

232 the fjord-head setting on tidal range is small. We have not included an uncertainty estimate in our

233 overall RSL reconstruction to reflect this, because the uncertainty in the proxy elevations is already of

234 a similar magnitude (±0.10-0.15 m, see Table S2 in Supplementary Information).

235

236 *2.3 Chronology*

237 To provide a chronology to constrain the timing of reconstructed RSL changes we use a range of

238 complementary methods to maximise the precision of the resultant age-depth model. Very low

239 concentrations of ^{210}Pb in the sediments required us to use other methods to provide recent

240 sedimentation rates. We investigated the presence of Total Mercury (Hg) (mg/kg, which includes both

241 mineral and atmospheric deposition) within the sediments using acid dissolution and quadrapole ICP-

242 MS as an indicator of anthropogenic emissions. Other studies in western and northern Greenland note

243 that between 1850-1900 CE there is more than a 2-fold increase in abundance of total Hg in lake

244 sediments compared to late Holocene levels (Bindler et al., 2001; Lindeberg et al., 2006; Shotyk et al.,

245 2003; Zheng, 2015), whereas Perez-Rodriguez et al. (2018) see a rapid increase in Hg abundance from

246 1880 onwards in southern Greenland. We therefore assume that the onset of detectable Hg above

247 background level in the Dronning Marie Dal saltmarsh sediments at 4-4.5 cm indicates an age of 1850-

248 1900 CE and use 1875 ± 25 CE in the age-depth modelling described below. For the earlier part of the

249 sediment record we submitted seeds and leaves from saltmarsh and nearby freshwater plants picked

250 from multiple horizons within the sediment for AMS ^{14}C dating at the [14]Chrono centre at Queen's

251 University, Belfast (Table 1). We generated an age-depth model for the whole sequence using the

252 *P_Sequence* approach with *variable k* in Oxcal v. 4.3 using the IntCal20 calibration curve (Bronk

253 Ramsey, 2009; Ramsey and Lee, 2013; Reimer et al., 2020). The resultant age-depth model uses the

254 Hg chronohorizon (1850-1900 CE) and three ^{14}C dates from lower in the sequence to estimate the age

255 of every 0.25 cm of sediment in the sediment section with associated uncertainty (Table 1 and Table S2

256 in supplementary information). The chronological uncertainty reported throughout this study is the

257 95% probability distribution (Bronk Ramsey, 2009).

258

259 We exclude the ^{14}C ages at 6-6.5 cm (UBA28477) and 9-9.5 cm (UBA28478) from the age-depth model

260 because they were on extremely small samples (<0.3 mg carbon) and are from samples that mix seeds

261 and leaves from high salt marsh with freshwater plants that would not have been growing close together

262 at the time (based on the palaeoenvironment recorded by the fossil diatom assemblage, and the

263 distribution of diatoms and vegetation types on the present-day saltmarsh) (Table 1). The dated

264 macrofossils from lower in the sequence are more likely to be autochthonous as the diatoms record a

265 high marsh to freshwater environment, close to HAT, at the time of deposition.

266

267 *Table 1. Radiocarbon dated samples from the Dronning Marie Dal saltmarsh core. Samples at 6-6.5*

268 *and 9-9.5 cm are not included in the chronology because they were on extremely small samples (<0.3*

269 *mg when graphitized) and mix seeds and leaves from different sources.*

270

Core depth (cm)	Lab number	^{14}C age (yr BP)	^{14}C age error (yr/1 sigma)	F^{14}C	F^{14}C error	Calibrated age yr CE (unmodelled)	Cal curve	Dated material	Used in age model?
6-6.5	UBA28477	Modern	n/a	1.0265	0.1421	n/a	n/a	Carex subspathacea seeds and Empetrum nigrum leaves	N
9-9.5	UBA28478	Modern	n/a	1.0107	0.0052	n/a	n/a	Carex subspathacea seeds and Empetrum nigrum leaves	N
Core depth (cm)	Lab number	^{14}C age (yr CE/BP)	^{14}C age error (yr/1 sigma)	F^{14}C	F^{14}C error		Cal curve	Dated material	Used in age model?
10-10.5 / 6-6.5	UBA28481 / UBA28477	208 BP / Modern	67 / n/a	n/a / 1.0265	n/a / 0.1421	1520-1950	INTCAL20 / n/a	Carex subspathacea seeds / Carex subspathacea seeds/Empetrum nigrum leaves	Y / N
11.5-12	UBA28476	134 BP	93	n/a	n/a	1528-1950	INTCAL20	Carex subspathacea seeds	Y
12-13 / 9-9.5	UBA28479 / UBA28478	44 BP / Modern	45 / n/a	0.99453 / 1.0107	0.00555 / 0.0052	1683-1930	INTCAL20 + NHZ1	Carex subspathacea seeds / Carex subspathacea seeds/Empetrum nigrum leaves	Y / N
10-10.5	UBA28481	208 BP	67	n/a	n/a		INTCAL20	Carex subspathacea seeds	Y
11.5-12	UBA28476	134 BP	93	n/a	n/a		INTCAL20	Carex subspathacea seeds	Y
12-13	UBA28479	44 BP	45	0.99453	0.00555		INTCAL20 + NHZ1	Carex subspathacea seeds	Y

271

2.4 Modelling RSL

2.4.1 Deglacial RSL change

There is a high degree of uncertainty on the rate of GIA in south-east Greenland, owing largely to the lack of Holocene RSL data points to constrain deglacial history. Marine ingression into an isolation basin at Timmiarmiut (100 km SW of Dronning Marie Dal) at c. 1140 CE (Table 2, also see Figures S1, S2 and Table S1 in the supplementary information) gives an empirical estimate of regional GIA and suggests that the linear rate of background RSL change over the past millennium is in the range of +0.2 to +0.8mm/yr (Table 2). We therefore use a mid-point value of +0.5 mm/yr as the rate of RSL change due to ongoing deglacial GIA in this study, rather than model predictions outlined in Section 2.1 which are not validated using RSL data from this region.

282

Table 2. Isolation basin sea-level index point from Timmiarmiut used to calculate the rate of RSL due

to ongoing GIA in this study.

Location (lat,lon)	Sill height (m MTL)	Reference Water Level	RSL (m)	Max cal age CE	Min cal age CE	Cal age error +/-	^{14}C age	Lab code
Timmiarmiut XC1403A (62.4987, -42.2577)	1.33 +/- 0.5	Ingression (MHWST to HAT)	-0.24 +/- 0.5	1044	1243	99.5	873 +/- 30	AAR 25631

285

286   2.4.2 Post Little Ice Age Greenland contribution

287   The post-LIA contribution to RSL at Dronning Marie Dal is computed using the sea level algorithm of

288   Kendall et al. (2005) computerised by Milne and Mitrovica (2003). This code computes the geoidal and

289   crustal response to ice and ocean loads on a spherically-symmetric Earth discretized into 25 km-thick

290   elastic layers as defined by Dziewonski and Anderson (1981), and three viscous layers comprising a

291   lithosphere, upper and lower mantle. Lithospheric thicknesses (L) in the range 71-120 km are

292   considered, with upper mantle (ν_{UM}) and lower mantle (ν_{LM}) viscosities of 0.1-1 x 10^{21} and 1-50 x 10^{21}

293   Pa s explored to quantify the effect on predicted RSL change of different assumptions about Earth

294   viscosity structure. The post-LIA ice history for the GrIS is derived from Kjeldsen et al. (2015) who

295   used a collection of aerial imagery from 1978-1987 CE to compare to historical trimlines assumed to

296   be indicative of a maximum LIA position of the ice sheet and use 1900 CE as a Greenland-wide year

297   of retreat from the maximum position, while acknowledging considerable local and regional

298   differences. The extrapolation method of point-scale changes in ice thickness over this time period to

299   the rest of the Greenland Ice Sheet is detailed in the methods section of Kjeldsen et al. (2015).

300

301   2.4.3 Contribution from Greenland glaciers

302   Changes in ice thickness in peripheral Greenland glaciers is determined in exactly the same way as the

303   post-LIA Greenland contribution. The peripheral Greenland glacier mass balance history is extracted

304   from Marzeion et al. (2015) and considered separately from the global glacier dataset (Section 2.4.4)

305   due to their proximity to the field site; the RSL response is computed as described in Section 2.4.2.

306

307   2.4.4 Contribution from global glaciers

308   We calculate the sea level contribution from global glaciers by first computing the global fingerprint

309   for a +1mm/yr barystatic contribution from glacier complexes defined in Marzeion et al. (2015, 2012)

310   since 1902. For the purposes of this calculation, we distribute the mass change across the glacierised

311   regions equally since the use of a 512 harmonic truncation masks sub 100 km-scale variability in ice

312   thickness change across regions outside of Greenland. Ice thickness change will vary internally to each

313   glacierised area, but the great distance between southeast Greenland and many of the sources of melt

314   means that the solution is insensitive to spatially inhomogeneous changes in ice thickness within the

315   source regions. Ice thickness changes for each of the global glacier complexes are discretized into

316   decadal loading intervals and the global sea level response is computed using the density configuration

317   in the Preliminary Reference Earth Model (PREM) (Dziewonski and Anderson, 1981). We use a

318   lithospheric thickness of 96 km to represent a global average applied to all glacial sites and omit the

319   viscous component from this calculation. Dronning Marie Dal is proximal to glacier sources in Iceland

320   and Baffin Bay so should display some level of sensitivity to ice loss distribution over these glacierised

321   areas. However, it is in the 'near field' with respect to both of these sites, and therefore the use of a

322   more realistic ice loss distribution in these areas (e.g. peripheral thinning) will reduce the relative sea-

323   level rise recorded in southeast Greenland. The influence of low-latitude glaciers is excluded from the

324   sea level fingerprint calculations, as the areas of mass loss are below the spatial resolution of the

325   fingerprinting code. This simplified method produces similar results that of Frederikse et al. (2020).

326

327   2.4.5 Contribution from the Antarctic Ice Sheet

328   Loss of ice mass from either East or West Antarctic Ice Sheets will produce a relatively uniform sea-

329   level change fingerprint over the northern Hemisphere (Bamber and Riva, 2010; Mitrovica et al., 2001).

330   Recent Antarctic Ice Sheet change (1992-present) is relatively well-documented and quantified

331   (Meredith et al., 2019) compared to the period represented by the RSL data in this study. However, a

332   recent study by Frederikse et al. (2020) that applied a Monte Carlo approach to balance the budget of

333   global sea-level rise since 1900 used estimates of 20th century Antarctic Ice Sheet mass balance obtained

334   from Adhikari et al. (2018) where the focus of mass loss throughout the 20th century is thought to be in

335   the West Antarctic Ice Sheet, amounting to a global sea-level change of 0.05 ±0.04 mm/yr. We use the

14

resulting ensemble from Frederikse et al's (2020) analysis to compute Antarctic Ice Sheet contribution

at Dronning Marie Dal.

2.4.6 Contribution from steric changes

To compute the contribution from salinity and temperature changes in the nearby ocean, the

Thermodynamic Equation of Sea Water (McDougall and Barker, 2011) (algorithm available here:

https://www.teos-10.org/) was applied to compute the steric height of the ocean. This uses a suite of

proximal monthly temperature-depth and salinity-depth profiles extracted from the CMIP6 database for

the 'historical' experiments covering the period 1850-2014. The 'historical' experiment was chosen to

produce timeseries of depth-dependant potential temperature and salinity because the experiment forms

part of the principal set of CMIP6 simulations, and the forcing datasets provided to the AOGCMs are

consistent with a set of atmospheric and ocean observations (Eyring et al., 2016). We use only one

configuration of the variant ID, which relates to initialisation time and procedure, specific model

physics and forcing (r1i1p1f1) across all AOGCMs considered (NASA-GISS-E2, CESM2, AWI,

CanESM5 and FGOALS). The model output from the CMIP6 database has a spatial resolution in the

range of 50-200 km, so we use profiles located within 300 km of Dronning Marie Dal to calculate an

average trend in steric height for the nearby ocean. The steric heights are computed to reference depth

levels of 500 m, 1000 m, 2000 m and 3000 m. Computing steric heights to different reference levels

allow us to determine which depth(s) in the ocean are contributing to steric height variability. Ivchenko

et al. (2008) determined that for the North Atlantic for the period 1996-2006, applying a reference level

of 1000-1500 m was sufficient to capture steric height variability, although this study provides trends

in steric height across the maximum depth level available by each model in the region proximal to

Dronning Marie Dal.

2.4.7 Terrestrial Water Storage

To estimate the contribution of changes in terrestrial water storage we utilise the ensemble of timeseries

of Frederikse et al. (2020) covering the time-period 1900-2018 CE. This dataset was compiled by

including the effects of natural variability in water reservoirs attributed to hemispheric-scale

atmospheric and ocean circulation changes (Humphrey and Gudmundsson, 2019), changes in storage

15

365 from dam building (Chao et al., 2008) and groundwater depletion activities (Döll et al., 2014; Wada et

366 al., 2016).

367

368 In the next section the results from the field work, RSL reconstruction and sea-level modelling are then

369 compared to better understand changes in mass balance and RSL over recent centuries in southeast

370 Greenland.

371

372 **3. Results**

373 *3.1 Modern diatom assemblages*

374 Diatoms are zoned by elevation across the upper part of the intertidal zone at Dronning Marie Dal, with

375 individual species providing useful information for reconstructing RSL. Above 2.2 m MTL (>0.34 m

376 above HAT) no diatoms were found in surface sediments, probably because the environment is too arid.

377 There is a distinctive assemblage containing *Pinnularia intermedia* (>10 % at HAT, increasing to ~55

378 % in the highest samples) which ends at ~2.2 m MTL. We use this as a proxy sea level indicator ~~and~~

379 to reconstruct palaeo-marsh surface elevation changes when we find ~~>10 % of~~ *Pinnularia intermedia*

380 either < 10 %, between 10-20 % and above 20 % in fossil counts (Figures 3A and B and Table S2 in

381 supplementary information). These zones are supplemented at lower elevations by a relatively narrow

382 assemblage zone in the high to low marsh where *Pinnularia intermedia* values are negligible, *Navicula*

383 *cinta* is >5 % and *Navicula salinarum* is not present (Figure 3A and Table S2 in supplementary

384 information). We find th~~is upper intertidal/supratidal~~ese diatom assemblage zones *~~Pinnularia~~*

385 *~~intermedia~~* ~~assemblage at~~ in every marsh we have studied in southeast and southwest Greenland and

386 use them~~it~~ to reconstruct RSL rather than using a transfer function approach as their~~its~~ precision is as

387 good as or better (*Pinnularia intermedia* is present in >15 marshes between 59° and 69° N in southwest

388 and southeast Greenland with a vertical range of 0.2-0.4 m; unpublished data and Long et al., 2012,

389 2010; Woodroffe and Long, 2010, 2009). ~~Where *Pinnularia intermedia* is <10 % in fossil sample~~

390 ~~assemblages we consider other species, particularly *Navicula cincta* which is present in greatest~~

391 ~~abundance in lower parts of the marsh, to reconstruct RSL (Table S2 in supplementary~~

392 ~~information).~~This approach also allows us to consider changes in other parameters (e.g. changes in these

16

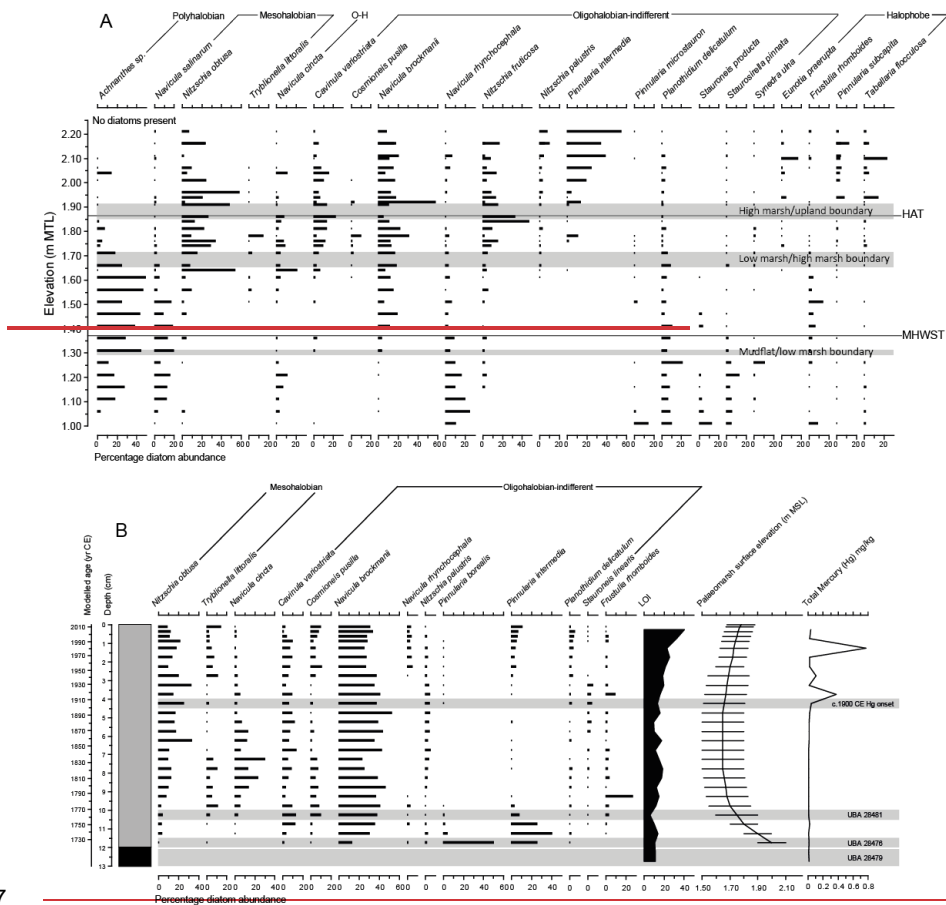393 species abundance between samples and sediment Loss on Ignition) when producing palaeo-marsh

394 surface elevation estimates.

395

396 *3.2 Core stratigraphy and biostratigraphy*

397 The core stratigraphy consists of a compacted basal freshwater organic silt-clay, grading upwards into

398 organic high saltmarsh sediments, and then into a slightly silt-rich organic low salt marsh towards the

399 surface, with an increase in LOI values ~~in the top 2 cm~~towards the surface (Figure 3B). Diatoms are

400 well preserved in the core and show a trend of falling palaeo-marsh surface elevation upwards from the

401 base of the sequence as *Pinnularia intermedia* declines and *Navicula cincta* increase~~s~~s in abundance

402 (alongside the absence of low marsh species *Navicula salinarum* which provides additional information

403 about palaeo-marsh surface elevations in this part of the core). In the top 3 cm *Pinnularia intermedia*

404 increases in abundance recording RSL beginning to fall and palaeo-marsh surface elevation increasing

405 (Figure 3B).

406

17

A

Polyhalobian — Mesohalobian — O-H — Oligohalobian-indifferent — Halophobe
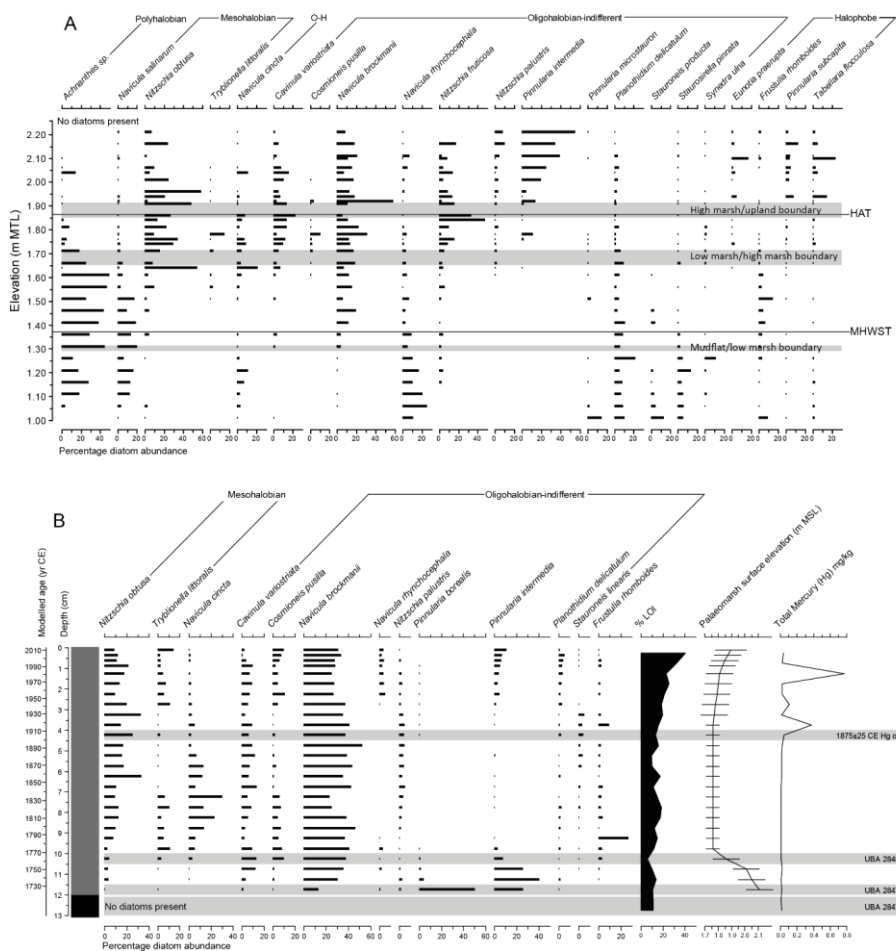

B

Figure 3. A) Modern diatom data from the marsh at Dronning Marie Dal. Data are expressed as % total diatom valves (%TDV). Only data >10% TDV are shown. B) Fossil diatom counts, palaeo-marsh surface elevation reconstruction and total Mercury measurements from the Dronning Marie Dal saltmarsh core. Diatoms are expressed as a %TDV and only taxa with >10% TDV are shown. Stratigraphy is shown in lefthand box where grey = saltmarsh sediment, black = freshwater peat. Total Mercury (mg/kg) was measured on salt marsh sediment using quadrapole ICP-MS.

3.3 RSL reconstructions

The saltmarsh sediments and diatoms indicate long term RSL rise. The rate of RSL rise at the start of the record (+~78 13 mm/yr between 1725-1762 CE; Figures 4B and C) is significantly higher than the

19

419 rate reconstructed from the closest isolation basin at Timmiarmiut (+0.5 ± 0.30.2-0.8 mm/yr; Table 2).

420 This may be due to LIA ice growth, including the nearby Skinfaxe glacier arm delivering sediment-

421 laden meltwater to Dronning Marie Dal, causing local ice loading and rapid infilling of accommodation

422 space and salt marsh development. The rate of RSL rise declines rapidly over the period 1762-1880

423 CE to +0.4 mm/yr and is within the error range of the isolation basin rate during most of this period

424 (+0.5 ± 0.30.3-3 mm/yr). This trend of rapid and then slowly rising RSL between 1725-1880 CE is

425 likely due to changes in the local LIA ice load over this time period combined with ongoing millennial-

426 scale GIA. The HUY3 model predicts +1.44 mm/yr of RSL rise over the past 1000 years in this region

427 (Lecavalier *et al.* 2014) which is larger than but the same sign as the salt marsh and isolation basin RSL

428 data during this period. Other recent estimates of centennial-scale GIA (Khan et al., 2016; van Dam et

429 al., 2017) suggest that RSL should have been falling over the past few hundred years at Dronning Marie

430 Dal. The isolation basin and salt marsh data instead suggest that RSL was rising or close to stable from

431 c. 1100 CE until c. 1880 CE.

432

433 Since 1880 CE RSL began to fall, which is indicated clearly in the diatom record by the decline in

434 *Navicula cincta* up core and the reintroduction and increasing abundance up core of *Pinnularia*

435 *intermedia*, a high marsh diatom species after 1900 CE (Figure 3B). There is ~0.09 ± 0.1 m of RSL fall

436 since 1880 CE, which if calculated as a constant rate of change is -0.72 ± 1.7 mm/yr RSL fall (Figures

437 4B and C, Table 3, Table S2 in supplementary information). Because of the lack of direct dating control

438 in upper part of the core and the slow rate of sedimentation it is not possible to infer decadal changes in

439 RSL rate during the 20th Century. This high marsh environment gives the most precise RSL

440 reconstructions and therefore we have the most confidence in the pattern of RSL during this recent part

441 of the record. RSL began to fall around 1880 CE at a relatively constant rate (< 1mm/yr) until the

442 1990s, when the rate of fall accelerates to between 1 and 3 mm/yr to present (2014 CE), resulting in

443 a total amount of RSL fall of -0.08 ±0.1 m since 1880 CE (Figures 4B and C, Table 3, Table S2 in
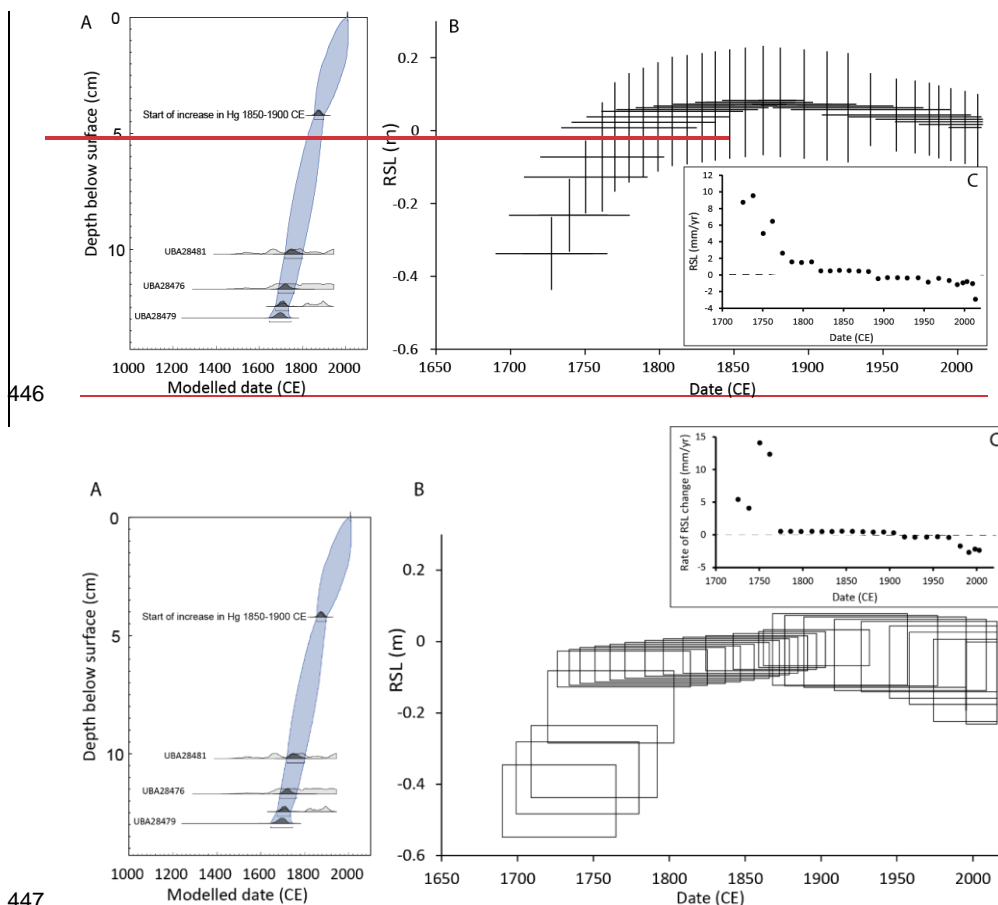
444 supplementary information).

445

Figure 4A) age-depth model using three ^{14}C ages and the Hg chrono-horizon, B) Dronning Marie Dal RSL curve, C) rates of RSL change through time inferred from the RSL and age data.

3.4 Modelled RSL changes

Published calculations of post LIA Greenland mass loss and other RSL contributors start at 1900 CE (e.g. Kjeldsen et al., 2015; Marzeion et al., 2015), so we focus on this part of the salt marsh RSL record to compare the reconstructed RSL with a modelled sea-level budget. The different contributions to the sea-level budget are summarised in Table 3 and Figure 5. For an average Earth model configuration of L = 96km, v_{UM} = 0.5 x 10^{21} Pa s and v_{LM} = 10 x 10^{21} Pa s, post-LIA ice mass loss (from the GrIS only) resulted in sea level change of –5.9 mm/yr at Dronning Marie Dal between 1900-2010 CE. Between 1983-2010 CE the modelled RSL rate was –10.1 mm/yr. Any chosen Earth configuration within the

parameter range explored does not significantly affect the predicted sea-level change; for 1900-2010 CE, the range of RSL fall was between –6.7 to –5.8mm/yr and 1983-2010 CE between -11.7 to -9.9 mm/yr. Using a fixed lithospheric thickness of 96km, the modelled total sea level fall arising from post-LIA mass loss across a suite of earth models with upper mantle viscosities ranging from $5 \times 10^{19} – 1 \times 10^{22}$ Pa s and lower mantle viscosities in the range of $1 \times 10^{21} – 5 \times 10^{22}$ Pa s was 0.65 to 0.86m, a difference of 0.21m which is within the uncertainty range of the RSL reconstruction (Figure 4B). The upper mantle viscosity is the largest contribution to this uncertainty accounting for both upper and lower bounds of this range. The effect of reducing the lithospheric thickness from 120km to 46km reduces the amount of modelled relative sea level fall by only a few cm. The contribution of peripheral Greenland glaciers to RSL was on average -1.7 ± 0.2 mm/yr between 1903 CE and present day; with decadal-scale contributions of -3 to -5 mm/yr between 1923 and 1943 CE. Global glacier mass loss contributes +0.24 ± 0.06 mm/yr RSL rise between 1903-2009 CE. Antarctica has contributed more significantly to sea-level change in recent years; for the period 1992 to 2016 CE, the Antarctic Peninsula and the West Antarctic Ice Sheet are thought to have resulted in +0.06 ± 0.73 mm/yr of barystatic sea-level change (Meredith et al., 2019). However, for the period 1850-2014 CE Frederikse et al. (2020) compute +0.088 ± 0.028 mm/yr, rising to +0.2mm/yr ± 0.05 mm/yr between 1970-2018 CE.

The range of values for the modelled steric contribution are in Table 4. They represent an upper estimate of the magnitude and range of the steric component as only profiles showing significant RSL trends are used when calculating the mean. From 1850-2014 CE, trends in steric height are in the range –0.23 to +0.18 mm/yr for a reference depth level of 1000 m and -0.36 to +0.28 mm/yr over a depth range of 2000 m. An observation-based analysis of trends in steric height by Frederikse et al. (2020) shows the steric contribution from the upper 2000m of the ocean close to Dronning Marie Dal between 1957-2018 CE is +0.13 mm/yr (we include steric trends derived for the period 1950-2014 in Table 4 for comparison). All models considered in Table 4 have larger values than Frederikse et al. (2020)'s estimates. Finally, the impact of terrestrial water storage amounts to a sea level fall of –0.13 ± 0.06 mm/yr at Dronning Marie Dal over the 20th century.

487 The different contributions to RSL are summed and plotted alongside the saltmarsh RSL data in Figure

488 5. The sum of components predicts RSL fall of between 0.58-0.93 m since 1900 CE. This prediction

489 is dominated by the contribution of GIA caused by post LIA Greenland and peripheral glacier mass

490 loss, which is only counteracted a little by the other components which mostly predict small amounts

491 of RSL rise. The saltmarsh data only reconstruct ~0.08 ±0.1 m of RSL fall since 1880 CE producing a

492 large mismatch between the sea-level budget and the saltmarsh RSL data. ~~However the RSL data does~~

493 ~~show an acceleration in the rate of RSL fall since the 1990s which agrees with accelerated GrIS mass~~

494 ~~loss in the 1983-2003 and 2003-2010 time periods in Kjeldsen et al. (2015).~~

495

496

497 *Table 3. Calculated amounts and rates of RSL change from the various contributors to the RSL budget*

498 *at Dronning Marie Dal. Rates of RSL change are supplied with ± 2-sigma uncertainty unless specified:*

499 ** uncertainty reflects assumed ± 10% error on rates which is larger than ± 2-sigma. ** steric sea level*

500 *contribution calculated from the average of significant trends for the 0-2000m depth interval from three*

501 *models in Table 4. *** GIA from nearby isolation basin ingression with uncertainty calculated from*

502 *upper and lower elevation reconstruction uncertainties.*

Contribution to sea-level budget	Local or global	Time period (CE)	Contribution to RSL change (mm), upper and lower estimates calculated for common period of 1900-2012 CE	Rate of RSL change (mm/yr) assumed for common period of 1900-2012 CE
GIA caused by post LIA ice mass loss*	Local	1900-2010	-724, -593	-5.9 ± 0.6
GIA caused by Greenland peripheral glacier mass change*	Local	1903-2012	-202, -166	-1.7 ± 0.2
Millennial-scale deglacial GIA***	Local	1900-2018	33, 88	+0.5 ± 0.3
Local total				**-7.1 ± 0.6 mm/yr**
Global glaciers	Global	1903-2012	20, 33	+0.24 ± 0.06
Antarctica	Global	1900-2018	0, 18	+0.08 ± 0.08
Steric**	Global	1850-2014	-39, 39	+0.00 ± 0.35
Terrestrial water storage	Global	1900-2018	-21, -8	-0.13 ± 0.06
Global total				**+0.19 ± 0.35 mm/yr**
Total modelled RSL change at Dronning Marie Dal 1900-2012 (see Figure 5)			-933, -589	-6.9 ± 1.5 mm/yr

Rate of RSL change from saltmarsh data (1880-2014)				-0.72~~67~~ ± 1.7 mm/yr

Table 4: Mean trends in steric height anomalies for three reference levels (500, 1000 and 2000m) calculated from profiles within 300km of Dronning Marie Dal using five models participating in the CMIP6 analysis. In all cases, experiment variant ID was r1i1p1f1. Numbers in brackets denote number of profiles displaying significant trends in steric height from which the mean and 2-sigma trends were calculated. The AWI model produced no significant trends for either time-period whilst GISS-E2 did not produce significant trends for 1850-2014 CE.

| Model ID	Resolution (space)	Resolution (time)	0-500m	0-1000m	0-2000m
1850-2014 CE					
GISS-E2	200km	Monthly	-	-	-
CESM2	100km	Monthly	0.08 ± 0.01 (34)	0.17 ± 0.01 (26)	0.09 ± 0.01 (7)
FGOALS	100km	Monthly	0.14 ± 0.12 (7)	0.18 ± 0.16 (11)	0.28 ± 0.04 (6)
AWI	25km	Decadal	-	-	-
CanESM5	100km	Monthly	-0.12 ± 0.1 (13)	-0.23 ± 0.08 (13)	-0.36 ± 0.06 (13)
1950-2014 CE					
GISS_E2	200km	Monthly	0.17 ± 0.02 (10)	0.36 ± 0.03 (6)	0.75 ± 0.05 (3)
CESM2	100km	Monthly	0.63 ± 0.15 (37)	1.3 ± 0.11 (26)	1.24 ± 0.07 (7)
FGOALS	100km	Monthly	0.43 ± 0.17 (11)	0.57 ± 0.18 (12)	0.81 ± 0.15 (6)
AWI	25km	Decadal	-	-	-
CanESM5	100km	Monthly	0.97 ± 0.34 (15)	1.1 ± 0.32 (13)	0.96 ± 0.2 (8)

514

515
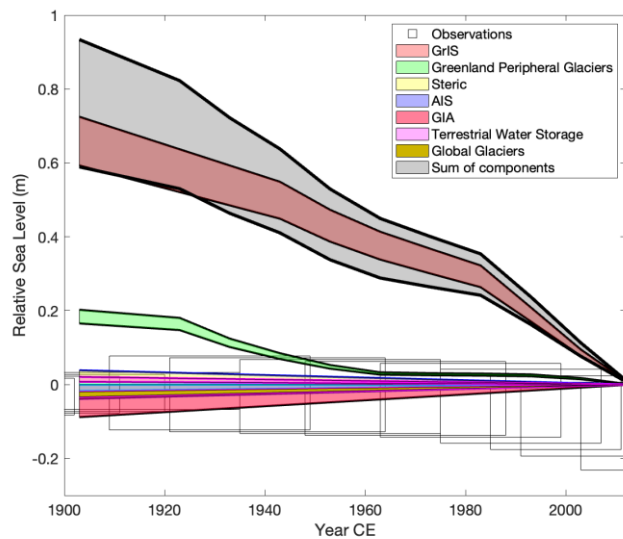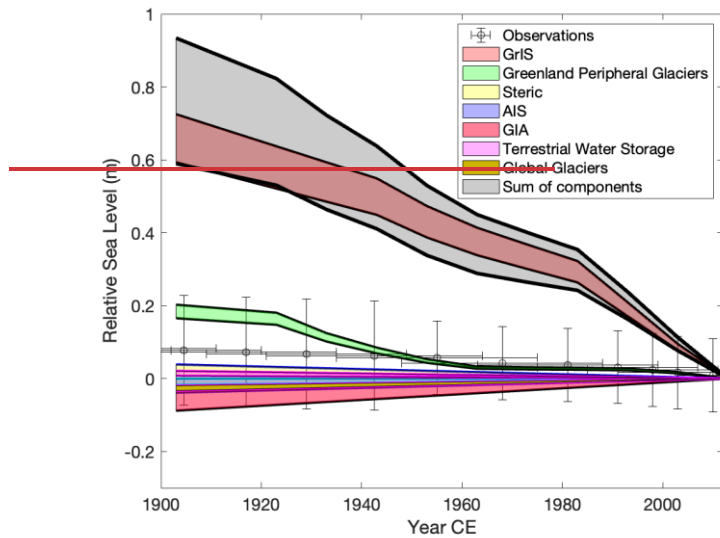
Figure 5: Observed and modelled relative sea level change from 1900-2010 CE as a function of recent

and late Holocene Greenland ice thickness changes (GIA caused by the GrIS, Greenland peripheral

glaciers and millennial-scale GIA; the 'local' signal) and from sources outside of Greenland (steric

signal, AIS, terrestrial water storage and global glaciers). The sum of the modelled components is

shown as the grey shaded area and the GrIS and peripheral glacier contributions are shown with an

estimated ±10% uncertainty. The black crosses are the salt marsh-based RSL reconstruction.

4. Discussion

The dominant contributors to post-LIA RSL change at Dronning Marie Dal are the adjustment of the solid Earth and changes in geoid height in response to both post-LIA and millennial-scale Greenland ice sheet changes. These contributors (ongoing GIA from the last deglaciation, post LIA Greenland mass balance and mass loss from peripheral Greenland glaciers) amount to a modelled sea-level fall of -7.1 mm/yr between 1900-2010 CE. By contrast, the RSL contributors unrelated to cryospheric change in Greenland only amount to modelled sea-level rise of +0.19 mm/yr, giving a total RSL fall of -6.9 mm/yr between the end of the LIA and present (Table 3). This clearly does not fit with the observations from the salt marsh data (Figures 4B, 5), which suggests that the rate of RSL fall between 1900-2013 CE is –0.72~~67~~ ± 1.7 mm/yr.

4.1 Timing of the end of the LIA and Greenland ice sheet and peripheral glacier contribution

To try to bring the post-LIA sea-level budget closer to the salt marsh observations, we explore two possible sources of uncertainty in the dominant post LIA Greenland signal: 1) timing of the start of post-LIA mass loss in Greenland and 2) greater uncertainty in modelled sea level associated with post-LIA GrIS and peripheral glacier mass loss.

To explore the possibility that the total post-LIA Greenland mass loss occurred over a longer time period we create five~~our~~ scenarios where the LIA maximum ice termination in Greenland is adjusted to begin at 1700, 1750, 1800, 1850 and 1900 CE, and the rate of mass loss is scaled accordingly with the end point remaining at 2010 (as in Kjeldsen et al., 2015). We know that the LIA ice sheet response was different around Greenland with multiple advance phases forced by different driving mechanisms, and it is simplistic to suggest that the whole of the ice sheet began to lose mass simultaneously at 1900 CE (Kjær et al., 2022), albeit it may serve as a Greenland-wide year. By adjusting the LIA termination date (and therefore the start of Greenland and peripheral glacier mass loss) we can investigate the impact of earlier ice retreat on RSL at Dronning Marie Dal. In this sensitivity analysis we recognise that moving

549   the LIA termination date in our modelling means that we are assuming the LIA ended simultaneously

550   earlier around the whole of Greenland, which is no more nuanced than assuming LIA termination at

551   1900 CE. We also note that the glaciers closest to Dronning Marie Dal appear to have been at their LIA

552   maximum position in the early 20th Century, which does not agree with an earlier LIA end in this

553   location (Bjork et al., 2012), and a recent alkenone-based sea-surface temperature reconstruction from

554   Nørre Skjoldungesund suggests considerable warming here occurred late, between c. 1915-1945 CE

555   (Wangner et al., 2020). The analysis does however allow a first-order investigation into the sensitivity

556   of modelled post-LIA sea level to the length of time over which the post-LIA mass loss occurred.

557

558   The second parameter that we vary as part of this sensitivity study is the total amount of post-LIA RSL

559   change mass loss from the GrIS and peripheral glaciers, by assuming an error of up to -30% on these

560   calculations. Kjeldsen et al. 2015 report uncertainties in their mass loss estimates for the Southeast

561   sector of the ice sheet between 7-15 %, and so this sensitivity analysis allows us to test the effect on

562   RSL at Dronning Marie Dal of a smaller amount of mass loss since the end of the LIA in this region.

563

564   Varying both LIA termination date and total post LIA mass loss from the GrIS and peripheral glaciers

565   affects has a large effect on how much sea-level change from other components is required to close the

566   post-LIA budget (Figure 6). The 'budget residual' in Figure 6 refers to the misfit in mm/yr between the

567   RSL change reconstructed by the saltmarsh data and RSL change predicted by the sea-level budget

568   calculations. In essence this is the amount of sea-level change that we still need to 'find' to close the

569   budget even after we modify the timing and total amount of mass loss from the dominant contributors

570   to RSL change of GrIS and peripheral glacier retreat since the end of the LIA.

571

572   The time-period over which post LIA mass loss occurs is important for understanding the degree of

573   volume mismatch between the RSL observations and modelled contributions from the maximum extent

574   to present. Figure 6a indicates that moving the LIA termination date from 1900 CE to 1700 50 CE reduces

575   the 'budget residual' required to fit the RSL data from ~+5.5 to ~+4 3.5 mm/yr. This residual is reduced

576   further (to ~+2.5 3 mm/yr) when considered alongside a 30% reduction in the amount of mass loss RSL

577   fall originating from the GrIS and peripheral glaciers compared to volumes reconstructed values

27

578 computed using RSL from ice histories generated by Kjeldsen et al. 2015 (GrIS) and Marzeion et al.

579 2015 (peripheral glaciers) (Figure 6b). Figures 6c and d further illustrate these results. Figure 6c, where

580 there is no reduction in the amount of post-LIA mass loss shows a ~~good~~ poor fit to the RSL data when

581 the LIA termination is moved to between 1700-1800 CE, ~~but~~ and there remains a +3.5 ~~-5~~ 4 mm/yr

582 'budget residual' which must be accounted for from other parts of the sea-level budget. In Figure 6d, a

583 ~~similar good~~ better fit to the RSL data is possible with a 30 % reduction in Greenland and peripheral

584 glacier mass-loss and LIA termination at 1800 CE. The remaining 'budget residual' is +3~~2.5~~ mm/yr

585 which again must be accounted for from other parts of the sea-level budget.

586

587 The smallest calculated 'budget residual' (~+3~~2.5~~ mm/yr) has to be found from processes causing sea-

588 level rise in southeast Greenland, such as millennial-scale Greenland GIA, Antarctic Ice Sheet melt, the

589 steric effect, and global glacier melt. The modelled sea-level budget suggests that these processes are

590 only small contributors to total sea-level change, with the sum of sources from outside Greenland only

591 +0.19 mm/yr since 1900 CE. The steric effect has the largest uncertainty, which we consider in Section

592 4.8 alongside other potential sources of error in our calculations. It is difficult however to see how the

593 contributors to RSL rise in southeast Greenland could be significantly larger before 1900 CE given the
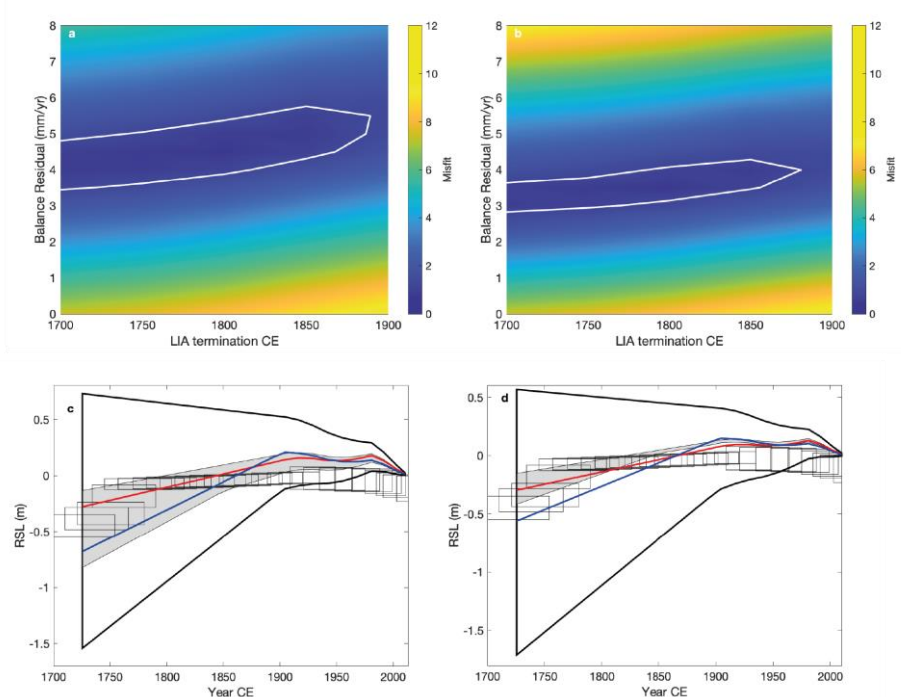
594 cooler regional temperatures of the LIA.

595

Figure 6. a, b) Misfit plots showing model data-fit where combinations of 'budget residuals' and LIA termination dates are considered with (a) no assumed error in the RSL contribution from the GrIS and (b) a 30 % reduction in magnitude of sea-level change associated with local changes in the GrIS. Areas within the white lines have a statistically equivalent fit to the RSL data, c) Modelled RSL from all combinations of LIA termination date and budget residual, assuming no error in the RSL contribution from the GrIS. Area within the black line denotes all possible combinations of RSL trends from LIA terminations from 1750-1900 CE and budget residual rates between 0-6mm/yr. Grey shaded area corresponds to RSL trends from within white lines on Figure 6a, demonstrating a statistically equivalent fit to the data. For illustrative purposes, the red line denotes a modelled RSL scenario with an LIA termination date of 1900 CE (assumed LIA termination date in Kjeldsen et al. 2015) and a budget residual rate of +4mm/yr and LIA termination date of 1800 CE; the blue line a modelled RSL scenario with a budget residual rate of +5mm/yr and LIA termination date of 1900 CE. d) As part c except grey shaded area corresponds to RSL trends from Figure 6b, demonstrating a statistically equivalent fit to the data. For illustrative purposes, the red line denotes a modelled RSL scenario with a budget residual

611 *rate of +~~2.5~~3mm/yr and LIA termination date of 1~~8~~700 CE; the blue line a modelled RSL scenario with*

612 *a budget residual rate of +~~5~~4mm/yr and LIA termination date of 1900 CE.*

613

614 *4.2   Reliability of saltmarsh RSL data*

615 Saltmarshes and their microfossil communities are widely used in temperate locations and previously

616 in west and south Greenland to reconstruct recent RSL changes with high precision (e.g. Kemp et al.,

617 2009, 2017; Long et al., 2012, 2010; Woodroffe and Long, 2009). At Dronning Marie Dal, the first

618 half of the RSL record (1725-1880 CE) is harder to interpret because early, rapid RSL rise may indicate

619 either a local LIA loading signal or a non RSL factor (e.g. sediment supply changes) as the marsh

620 became established. What we can say with certainty is that RSL began to fall at or soon after 1880 CE,

621 suggesting additional contributors to RSL or changes in the dominance of existing contributors caused

622 this change in the sign and rate of RSL. We are also confident of the total amount of RSL fall between

623 1880 CE and present, which is less than predicted by any permutation of the sea-level budget modelling

624 (Figure 5). We acknowledge however that these reconstructions come from a single sediment core and

625 although the stratigraphy appeared consistent across the marsh during fieldwork it would be ideal to

626 replicate these results within another core from the same marsh and also from other marshes close to

627 the ice sheet margin in this region in the future.

628

629 There is no indication of hiatuses within the marsh sediment and based on surveys of modern marshes

630 here and elsewhere in Greenland the elevation range of the key diatom species *Pinnularia intermedia*

631 used in the palaeo-marsh surface elevation calculations is robust. A RSL fall of ~0.6-0.9 m since 1900

632 CE as predicted by the sea-level budget modelling, would have lifted what was a high marsh

633 environment at the start of the period (indicated by the taxa at ~5 cm depth, Figure 3B) out of the

634 intertidal and into the adjacent freshwater zone where diatoms are not preserved due to extreme aridity.

635 The continuous preservation of intertidal diatoms through the sediment sequence to the surface where

636 modern saltmarsh plants were growing during sampling (Figure 2) rules out this possibility. Even the

637 smaller amount of RSL fall (~0.2 m) since 1900 CE predicted by an earlier LIA termination date (1800

638 CE) and 30% smaller GrIS contribution (Figure 6) is unlikely because the diatoms suggest a mid-high

639 marsh environment at 1900 CE and the core top elevation is within the high marsh zone, a vertical

640 distance based on analysis of modern diatoms at Dronning Marie Dal of ~0.1 m, which is half of the

641 predicted RSL fall (~0.2 m). Greenland saltmarshes accrete very slowly and only record sustained RSL

642 changes over decades, and therefore short-timescale variability in contributors (e.g. due to decadal

643 temperature fluctuations in the 20th Century) is not distinguishable in the saltmarsh data. However, the

644 total amount of RSL fall and the timing of the change from RSL rise/stability to RSL fall is robustly

645 reconstructed and we are confident that this provides an important test of Greenland RSL modelling.

646

647 *4.3 Limitations of RSL modelling*

648 Regional sea level budgets deviate significantly from the global budget, are challenging to compute and

649 have been deemed part of the 'Regional Sea-Level Change and Coastal Impacts' Grand Challenge by

650 the World Climate Research Programme (WCRP, 2022). Of the different items in the sea-level budget

651 for Dronning Marie Dal, the large uncertainty in the steric contribution could potentially be the source

652 of additional sea-level rise which would help decrease the 'budget residual' identified in Figure 6. The

653 data in Table 4 do not fully capture the range of uncertainty in the steric component of sea level. These

654 uncertainties arise from poor to non-existent capture of the dynamics of coastal regions, namely the

655 propagation of the change in steric height of the open ocean to the fjord location and the lack of

656 observations to constrain model output in the early 20th Century.

657

658 The field site is located at the head of the 50 km long marine fjord Søndre Skoldungesund and therefore

659 the steric contribution may be different to that calculated from the open ocean estimates within 300 km

660 of Dronning Marie Dal averaged in this study. A multibeam study of the fjord by Kjeldsen et al. (2017)

661 shows the fjord is between 1.1-3.1 km wide, up to 800 m deep in the outer part, with a shallow (77m

662 deep) sill at mid-fjord and shallow depths inside the sill. The fjord water is cold to the base along its

663 length, with no apparent intrusion of warmer Atlantic water from the shelf edge. The mixed predictions

664 of steric height changes from the different models suggest that this region is poorly constrained within

665 global steric datasets (Table 4). Given the lack of intrusion of warm Atlantic water into the fjord today

666 it is unlikely that there has been a more positive contribution of steric height from 20th Century warming.

667 However, with significant mass loss from the Greenland Ice Sheet since the LIA and an influx of cold

668   yet low-salinity meltwater into the fjord it is possible that the local halosteric component is

669   underestimated.

670

671   A second issue with the steric height calculation is the potential for the CMIP6 models to misrepresent

672   changes in the dynamic height of the ocean caused by shifts in the location of ocean currents, such as

673   the East Greenland Current (EGC) over time. A recent study of North Atlantic dynamic sea level and

674   its response to GrIS meltwater and temperature increase indicates general Atlantic Meridional

675   Overturning Circulation decline and increase in sea-surface height with increased GrIS melting, but the

676   response of the cold EGC is complex and in southeast Greenland the effect of warming and increased

677   meltwater on sea-surface height is minimal (Saenko et al., 2017). Given that Kjeldsen et al. (2017)

678   suggest the EGC does not currently penetrate into the Søndre Skoldungesund fjord the impact of any

679   dynamical changes in the EGC since the LIA are likely to be minor.

680

681   A third possible source of uncertainty in the sea-level budget is the application of the sea level code

682   used to calculate GIA, specifically the spectral resolution with which the algorithm predicts the sea

683   level response to loading increments. The mass balance history from Kjeldsen et al. (2015) is presented

684   on a 1x1 km spatial grid, but the sea level code utilises a spectral harmonic truncation of 256. The

685   effects on predicted RSL of the reduction in resolution has been demonstrated previously with near-

686   field relative sea level being more affected by harmonic truncation than far field sites (Spada and Melini,

687   2019). A move towards a higher degree spherical harmonic truncation (>1024) would be necessary to

688   faithfully reproduce sea level fingerprint histories associated with small outlet glaciers and should be

689   considered in the future (Adhikari et al., 2015).

690

691   Despite the limitations outlined above, this study presents a first test of a post-LIA sea-level budget in

692   the nearfield location of southeast Greenland. There is clear and unexplained difference between the

693   RSL history recorded by salt marsh sediments (a small RSL fall since the end of the LIA) and the RSL

694   budget which suggests significant RSL fall during this period. The sensitivity tests show that the budget

695   can fit the salt marsh RSL data if the amount of mass loss from the GrIS and peripheral glaciers is less,

696   and it took place over a longer period (Figure 6d), but even so a +2.5 mm/yr unexplained 'budget

697 residual' remains. RSL reconstructions from salt marshes in southwest Greenland (Long et al., 2012,

698 2010; Woodroffe and Long, 2010, 2009) also suggest that the dominant signal in southern Greenland is

699 RSL rise into the 20th Century, which correlates with the long term (pre ~1880 CE) trend of RSL rise at

700 Dronning Marie Dal.

701

702 **5. Conclusions**

703 Saltmarsh sediments collected at the mouth of Dronning Marie Dal, close to the GrIS margin in

704 southeast Greenland, record RSL changes over the past c. 300 years in changing sediment and diatom

705 stratigraphy.   These RSL changes record a combination of processes that are dominated by

706 local/regional changes in GrIS mass balance during this critical period that spans the maximum of the

707 LIA and 20th Century warming.

708

709 In the early part of the record (1725-1762 CE) the rate of RSL rise is higher than reconstructed from

710 the closest isolation basin at Timmiarmiut, but between 1762-1880 CE the rate decreases to within the

711 error range of the isolation basin RSL rate. This trend is likely due to changes in the local LIA ice load

712 over this time period combined with ongoing millennial-scale GIA, or other local processes as the salt

713 marsh is established. Other recent estimates of centennial-scale GIA (Khan et al., 2016; van Dam et

714 al., 2017) suggest that RSL should have been falling over the past few hundred years at Dronning Marie

715 Dal. The isolation basin and salt marsh data instead suggest that RSL was rising or close to stable from

716 c. 1100 CE until c. 1880 CE. RSL begins to slowly fall around 1880 CE and the rate then accelerates

717 from the 1990s, with a total amount of RSL fall of 0.098 ± 0.1 m since 1880 CE.

718

719

720

721

722 Modelled RSL, which takes into account contributions from post-LIA GrIS GIA, ongoing deglacial

723 GIA, the global non-ice sheet glacial fingerprint, the contribution from thermosteric effects, an estimate

724 of the Antarctic fingerprint and the contribution from terrestrial water storage, over-predicts the amount

725 of RSL fall since the end of the LIA by at least 0.5 m. The GIA signal caused by post-LIA GrIS mass

726 loss is by far the largest contributor, and error in its calculation has the largest potential to impact RSL

727 predictions at Dronning Marie Dal. We cannot reconcile the modelled contributions and the saltmarsh

728 observations, even when moving the termination of the LIA to 1~~78~~00 CE, and reducing the post-LIA

729 Greenland mass loss signal by 30%. A 'budget residual' of ~+~~2.5~~3 mm/yr since the end of the LIA

730 remains unexplained. Explaining the difference between salt marsh RSL data and the modelled RSL

731 budget since the end of the LIA and determining the timing of the LIA termination should be a key

732 future research objectives which can be addressed through reducing uncertainty on each component to

733 the sea-level budget, collecting more empirical data on the recent history of the GrIS and by replicating

734 the salt marsh RSL record presented here elsewhere in this and other regions of Greenland.

735

736 *Author Contribution*

737 SAW, LMW, AJL and KKK designed the study, SAW, KKK and KHK undertook fieldwork, NLMB

738 undertook the laboratory analysis, and SAW and LMW prepared the manuscript with contributions

739 from all co-authors.

740

741 The authors declare that they have no conflict of interest.

742

753

754 Adhikari, S., Ivins, E. R., and Larour, E.: ISSM-SESAW v1.0: mesh-based computation of
755 gravitationally consistent sea level and geodetic signatures caused by cryosphere and
756 climate driven mass change, Climate and Earth System Modeling,
757 https://doi.org/10.5194/gmdd-8-9769-2015, 2015.

758 Adhikari, S., Caron, L., Steinberger, B., Reager, J. T., Kjeldsen, K. K., Marzeion, B., Larour,
759 E., and Ivins, E. R.: What drives 20th century polar motion?, Earth Planet. Sci. Lett., 502,
760 126–132, https://doi.org/10.1016/j.epsl.2018.08.059, 2018.

761 Adhikari, S., Milne, G. A., Caron, L., Khan, S. A., Kjeldsen, K. K., Nilsson, J., Larour, E., and
762 Ivins, E. R.: Decadal to Centennial Timescale Mantle Viscosity Inferred from Modern Crustal
763 Uplift Rates in Greenland, Geophys. Res. Lett., n/a, e2021GL094040,
764 https://doi.org/10.1029/2021GL094040, 2021.

765 Allen, J. R. L.: Morphodynamics of Holocene salt marshes: a review sketch from the Atlantic
766 and Southern North Sea coasts of Europe, Quat. Sci. Rev., 19, 1155–1231,
767 https://doi.org/Doi 10.1016/S0277-3791(99)00034-7, 2000.

768 Bamber, J. and Riva, R.: The sea level fingerprint of recent ice mass fluxes, The
769 Cryosphere, 4, 621–627, https://doi.org/10.5194/tc-4-621-2010, 2010.

770 Barlow, N. L. M., Shennan, I., Long, A. J., Gehrels, W. R., Saher, M. H., Woodroffe, S. A.,
771 and Hillier, C.: Salt marshes as late Holocene tide gauges, Glob. Planet. Change, 106, 90–
772 110, https://doi.org/10.1016/j.gloplacha.2013.03.003, 2013.

773 Bevis, M., Wahr, J., Khan, S. A., Madsen, F. B., Brown, A., Willis, M., Kendrick, E., Knudsen,
774 P., Box, J. E., van Dam, T., Caccamise, D. J., Johns, B., Nylen, T., Abbott, R., White, S.,
775 Miner, J., Forsberg, R., Zhou, H., Wang, J., Wilson, T., Bromwich, D., and Francis, O.:
776 Bedrock displacements in Greenland manifest ice mass variations, climate cycles and
777 climate change, Proc. Natl. Acad. Sci. U. S. A., 109, 11944–11948, https://doi.org/DOI
778 10.1073/pnas.1204664109, 2012.

779 Bevis, M., Harig, C., Khan, S. A., Brown, A., Simons, F. J., Willis, M., Fettweis, X., Broeke,
780 M. R. van den, Madsen, F. B., Kendrick, E., Caccamise, D. J., Dam, T. van, Knudsen, P.,
781 and Nylen, T.: Accelerating changes in ice mass within Greenland, and the ice sheet's
782 sensitivity to atmospheric forcing, Proc. Natl. Acad. Sci., 116, 1934–1939,
783 https://doi.org/10.1073/pnas.1806562116, 2019.

784 Bindler, R., Renberg, I., Appleby, P. G., Anderson, N. J., and Rose, N. L.: Mercury
785 Accumulation Rates and Spatial Patterns in Lake Sediments from West Greenland: A Coast
786 to Ice Margin Transect, Environ. Sci. Technol., 35, 1736–1741,
787 https://doi.org/10.1021/es0002868, 2001.

788 Bjork, A. A., Kjaer, K. H., Korsgaard, N. J., Khan, S. A., Kjeldsen, K. K., Andresen, C. S.,
789 Box, J. E., Larsen, N. K., and Funder, S.: An aerial view of 80 years of climate-related glacier
790 fluctuations in southeast Greenland, Nat. Geosci., 5, 427–432,
791 https://doi.org/10.1038/Ngeo1481, 2012.

792 Briner, J. P., Young, N. E., Thomas, E. K., Stewart, H. A. M., Losee, S., and Truex, S.: Varve
793 and radiocarbon dating support the rapid advance of Jakobshavn Isbræ during the Little Ice
794 Age, Quat. Sci. Rev., 30, 2476–2486, https://doi.org/10.1016/j.quascirev.2011.05.017, 2011.

795 Briner, J. P., Cuzzone, J. K., Badgeley, J. A., Young, N. E., Steig, E. J., Morlighem, M.,
796 Schlegel, N.-J., Hakim, G. J., Schaefer, J. M., Johnson, J. V., Lesnek, A. J., Thomas, E. K.,
797 Allan, E., Bennike, O., Cluett, A. A., Csatho, B., de Vernal, A., Downs, J., Larour, E., and
798 Nowicki, S.: Rate of mass loss from the Greenland Ice Sheet will exceed Holocene values
799 this century, Nature, 586, 70–74, https://doi.org/10.1038/s41586-020-2742-6, 2020.

800 van den Broeke, M., Bamber, J., Ettema, J., Rignot, E., Schrama, E., van de Berg, W., van
801 Meijgaard, E., Velicogna, I., and Wouters, B.: Partitioning Recent Greenland Mass Loss,
802 Science, 326, 984–986, https://doi.org/10.1126/science.1178176, 2009.

803 Bronk Ramsey, C.: Bayesian analysis of radiocarbon dates, Radiocarbon, 51, 337–360,
804 2009.

805 Chao, B. F., Wu, Y. H., and Li, Y. S.: Impact of Artificial Reservoir Water Impoundment on
806 Global Sea Level, Science, 320, 212–214, https://doi.org/10.1126/science.1154580, 2008.

807 Chen, G., Zhang, S., Liang, S., and Zhu, J.: Elevation and Volume Changes in Greenland
808 Ice Sheet From 2010 to 2019 Derived From Altimetry Data, Front. Earth Sci., 9, 674983,
809 https://doi.org/10.3389/feart.2021.674983, 2021.

810 Chylek, P., Dubey, M. K., and Lesins, G.: Greenland warming of 1920-1930 and 1995-2005,
811 Geophys. Res. Lett., 33, https://doi.org/Artn L11707 10.1029/2006gl026510, 2006.

812 van Dam, T., Francis, O., Wahr, J., Khan, S. A., Bevis, M., and van den Broeke, M. R.: Using
813 GPS and absolute gravity observations to separate the effects of present-day and
814 Pleistocene ice-mass changes in South East Greenland, Earth Planet. Sci. Lett., 459, 127–
815 135, https://doi.org/10.1016/j.epsl.2016.11.014, 2017.

816 Döll, P., Müller Schmied, H., Schuh, C., Portmann, F. T., and Eicker, A.: Global-scale
817 assessment of groundwater depletion and related groundwater abstractions: Combining
818 hydrological modeling with information from well observations and GRACE satellites, Water
819 Resour. Res., 50, 5698–5720, https://doi.org/10.1002/2014WR015595, 2014.

820 Dyke, L. M., Hughes, A. L. C., Murray, T., Hiemstra, J. F., Andresen, C. S., and Rodés, Á.:
821 Evidence for the asynchronous retreat of large outlet glaciers in southeast Greenland at the
822 end of the last glaciation, Quat. Sci. Rev., 99, 244–259,
823 https://doi.org/10.1016/j.quascirev.2014.06.001, 2014.

824 Dyke, L. M., Hughes, A. L., Andresen, C. S., Murray, T., Hiemstra, J. F., Bjørk, A. A., and
825 Rodés, Á.: The deglaciation of coastal areas of southeast Greenland, The Holocene, 28,
826 1535–1544, https://doi.org/10.1177/0959683618777067, 2018.

827 Dziewonski, A. M. and Anderson, D. L.: Preliminary reference Earth model, Phys. Earth
828 Planet. Inter., 25, 297–356, https://doi.org/10.1016/0031-9201(81)90046-7, 1981.

829 Eyring, V., Bony, S., Meehl, G. A., Senior, C. A., Stevens, B., Stouffer, R. J., and Taylor, K.
830 E.: Overview of the Coupled Model Intercomparison Project Phase 6 (CMIP6) experimental
831 design and organization, Geosci. Model Dev., 9, 1937–1958, https://doi.org/10.5194/gmd-9-
832 1937-2016, 2016.

833 Farrell, W. E. and Clark, J. A.: On Postglacial Sea Level, Geophys. J. R. Astron. Soc., 46,
834 647–667, https://doi.org/10.1111/j.1365-246X.1976.tb01252.x, 1976.

835 Frederikse, T., Landerer, F., Caron, L., Adhikari, S., Parkes, D., Humphrey, V. W.,
836 Dangendorf, S., Hogarth, P., Zanna, L., Cheng, L., and Wu, Y.-H.: The causes of sea-level
837 rise since 1900, Nature, 584, 393–397, https://doi.org/10.1038/s41586-020-2591-3, 2020.

838 Funder, S. and Hansen, L.: The Greenland ice sheet - a model for its culmination and decay
839 during and after the last glacial maximum, Bull. Geol. Soc. Den., 42, 137–152, 1996.

840 Funder, S., Kjeldsen, K. K., Kjaer, K. H., and O Cofaigh, C.: The Greenland Ice Sheet during
841 the last 300,000 years: a review, Dev. Quat. Sci., 15, 699-713. doi: 10.1016/B978-0-444-
842 53447-7.00050-7, 2011.

Hughes, A., Rainsley, E., Murray, T., Fogwill, C., Schnabel, C., and Xu, S.: Rapid response of Helheim Glacier, southeast Greenland, to early Holocene climate warming, Geology, 40, 427–430, https://doi.org/10.1130/G32730.1, 2012.

Humphrey, V. and Gudmundsson, L.: GRACE-REC: a reconstruction of climate-driven water storage changes over the last century, Earth Syst. Sci. Data, 11, 1153–1170, https://doi.org/10.5194/essd-11-1153-2019, 2019.

Ivchenko, V. O., Danilov, S., Sidorenko, D., Schröter, J., Wenzel, M., and Aleynik, D. L.: Steric height variability in the Northern Atlantic on seasonal and interannual scales, J. Geophys. Res., 113, C11007, https://doi.org/10.1029/2008JC004836, 2008.

Kemp, A., Horton, B., Culver, S., Corbett, D., van de Plassche, O., Gehrels, W., Douglas, B., and Parnell, A.: Timing and magnitude of recent accelerated sea-level rise (North Carolina, United States), Geology, 37, 1035–1038, https://doi.org/10.1130/G30352A.1, 2009.

Kemp, A. C., Kegel, J. J., Culver, S. J., Barber, D. C., Mallinson, D. J., Leorri, E., Bernhardt, C. E., Cahill, N., Riggs, S. R., Woodson, A. L., Mulligan, R. P., and Horton, B. P.: Extended late Holocene relative sea-level histories for North Carolina, USA, Quat. Sci. Rev., 160, 13–30, https://doi.org/10.1016/j.quascirev.2017.01.012, 2017.

Kendall, R. A., Mitrovica, J. X., and Milne, G. A.: On post-glacial sea level - II. Numerical formulation and comparative results on spherically symmetric models, Geophys. J. Int., 161, 679–706, https://doi.org/10.1111/j.1365-246X.2005.02553.x, 2005.

Khan, S. A., Aschwanden, A., Bjork, A. A., Wahr, J., Kjeldsen, K. K., and Kjaer, K. H.: Greenland ice sheet mass balance: a review, Rep. Prog. Phys., 78, 26, https://doi.org/10.1088/0034-4885/78/4/046801, 2015.

Khan, S. A., Sasgen, I., Bevis, M., van Dam, T., Bamber, J. L., Wahr, J., Willis, M., Kjaer, K. H., Wouters, B., Helm, V., Csatho, B., Fleming, K., Bjork, A. A., Aschwanden, A., Knudsen, P., and Munneke, P. K.: Geodetic measurements reveal similarities between post-Last Glacial Maximum and present-day mass loss from the Greenland ice sheet, Sci. Adv., 2, https://doi.org/ARTN e1600931 10.1126/sciadv.1600931, 2016.

Khan, S. A., Bjørk, A. A., Bamber, J. L., Morlighem, M., Bevis, M., Kjær, K. H., Mouginot, J., Løkkegaard, A., Holland, D. M., Aschwanden, A., Zhang, B., Helm, V., Korsgaard, N. J., Colgan, W., Larsen, N. K., Liu, L., Hansen, K., Barletta, V., Dahl-Jensen, T. S., Søndergaard, A. S., Csatho, B. M., Sasgen, I., Box, J., and Schenk, T.: Centennial response of Greenland's three largest outlet glaciers, Nat. Commun., 11, 5718, https://doi.org/10.1038/s41467-020-19580-5, 2020.

Kjær, K. H., Bjørk, A. A., Kjeldsen, K. K., Hansen, E. S., Andresen, C. S., Siggaard-Andersen, M.-L., Khan, S. A., Søndergaard, A. S., Colgan, W., Schomacker, A., Woodroffe, S., Funder, S., Rouillard, A., Jensen, J. F., and Larsen, N. K.: Glacier response to the Little Ice Age during the Neoglacial cooling in Greenland, Earth-Sci. Rev., 227, 103984, https://doi.org/10.1016/j.earscirev.2022.103984, 2022.

Kjeldsen, K., Korsgaard, N., Bjork, A., Khan, S., Box, J., Funder, S., Larsen, N., Bamber, J., Colgan, W., van den Broeke, M., Siggaard-Andersen, M., Nuth, C., Schomacker, A., Andresen, C., Willerslev, E., and Kjaer, K.: Spatial and temporal distribution of mass loss from the Greenland Ice Sheet since AD 1900, Nature, 528, 396–400, https://doi.org/10.1038/nature16183, 2015.

Kjeldsen, K. K., Weinrebe, R. W., Bendtsen, J., Bjørk, A. A., and Kjær, K. H.: Multibeam bathymetry and CTD measurements in two fjord systems in southeastern Greenland, Earth Syst. Sci. Data, 9, 589–600, https://doi.org/10.5194/essd-9-589-2017, 2017.

889 Lecavalier, B., Milne, G. A., Simpson, M. J. R., Wake, L. M., Huybrechts, P., Tarasov, L.,
890 Kjeldsen, K. K., Funder, S. V., Long, A. J., Woodroffe, S. A., Dyke, A., and Larsen, N. K.: A
891 model of Greenland ice sheet deglaciation based on observations of relative sea-level and
892 ice extent, Quat. Sci. Rev., in press, 2014.

893 Lepping, O. and Daniëls, F. J. A.: Phytosociology of Beach and Salt Marsh Vegetation in
894 Northern West Greenland, Polarforschung, 76, 95–108, 2007.

895 Levy, L. B., Larsen, N. K., Knudsen, M. F., Egholm, D. L., Bjørk, A. A., Kjeldsen, K. K., Kelly,
896 M. A., Howley, J. A., Olsen, J., Tikhomirov, D., Zimmerman, S. R. H., and Kjær, K. H.: Multi-
897 phased deglaciation of south and southeast Greenland controlled by climate and
898 topographic setting, Quat. Sci. Rev., 242, 106454,
899 https://doi.org/10.1016/j.quascirev.2020.106454, 2020.

900 Lindeberg, C., Bindler, R., Renberg, I., Emteryd, O., Karlsson, E., and Anderson, N. J.:
901 Natural Fluctuations of Mercury and Lead in Greenland Lake Sediments, Environ. Sci.
902 Technol., 40, 90–95, https://doi.org/10.1021/es051223y, 2006.

903 Long, A. J., Woodroffe, S. A., Milne, G. A., Bryant, C. L., and Wake, L. M.: Relative sea-level
904 change in West Greenland during the last millennium, Quat. Sci. Rev., 29, 367–383, 2010.

905 Long, A. J., Woodroffe, S. A., Milne, G. A., Bryant, C. L., Simpson, M. J. R., and Wake, L.
906 M.: Relative sea-level change in Greenland during the last 700 yrs and ice sheet response to
907 the Little Ice Age, Earth Planet. Sci. Lett., 315, 76–85, https://doi.org/DOI
908 10.1016/j.epsl.2011.06.027, 2012.

909 Marzeion, B., Jarosch, A. H., and Hofer, M.: Past and future sea-level change from the
910 surface mass balance of glaciers, The Cryosphere, 6, 1295–1322, https://doi.org/10.5194/tc-
911 6-1295-2012, 2012.

912 Marzeion, B., Leclercq, P. W., Cogley, J. G., and Jarosch, A. H.: Brief Communication:
913 Global reconstructions of glacier mass change during the 20th century are consistent, The
914 Cryosphere, 9, 2399–2404, https://doi.org/10.5194/tc-9-2399-2015, 2015.

915 McDougall, T. J. and Barker, P. M.: Getting started with TEOS-10 and the Gibbs Seawater
916 (GSW) Oceanographic Toolbox., 2011.

917 Meredith, M., Sommerkorn, M., Cassotta, S., Derksen, C., Ekaykin, A., Hollowed, A.,
918 Kofinas, G., Mackintosh, A., Melbourne-Thomas, J., Muelbert, M. M. C., Ottersen, G.,
919 Pritchard, H., and Schuur, E. A. G.: Polar Regions, in: IPCC Special Report on the Ocean
920 and Cryosphere in a Changing Climate, Cambridge University Press, 203–320, 2019.

921 Mitrovica, J. X. and Milne, G. A.: On post-glacial sea level: I. General theory, Geophys. J.
922 Int., 154, 253–267, https://doi.org/DOI 10.1046/j.1365-246X.2003.01942.x, 2003.

923 Mitrovica, J. X., Tamisiea, M. E., Davis, J. L., and Milne, G. A.: Recent mass balance of
924 polar ice sheets inferred from patterns of global sea-level change, Nature, 409, 1026–1029,
925 https://doi.org/10.1038/35059054, 2001.

926 Moon, T., Joughin, I., Smith, B., and Howat, I.: 21st-Century Evolution of Greenland Outlet
927 Glacier Velocities, Science, 336, 576–578, https://doi.org/10.1126/science.1219985, 2012.

928 Morlighem, M., Williams, C. N., Rignot, E., An, L., Arndt, J. E., Bamber, J. L., Catania, G.,
929 Chauché, N., Dowdeswell, J. A., Dorschel, B., Fenty, I., Hogan, K., Howat, I., Hubbard, A.,
930 Jakobsson, M., Jordan, T. M., Kjeldsen, K. K., Millan, R., Mayer, L., Mouginot, J., Noël, B. P.
931 Y., O'Cofaigh, C., Palmer, S., Rysgaard, S., Seroussi, H., Siegert, M. J., Slabon, P., Straneo,
932 F., van den Broeke, M. R., Weinrebe, W., Wood, M., and Zinglersen, K. B.: BedMachine v3:
933 Complete Bed Topography and Ocean Bathymetry Mapping of Greenland From Multibeam

934 Echo Sounding Combined With Mass Conservation, Geophys. Res. Lett., 44, 11,051-
935 11,061, https://doi.org/10.1002/2017GL074954, 2017.

936 Pérez-Rodríguez, M., Silva-Sánchez, N., Kylander, M. E., Bindler, R., Mighall, T. M.,
937 Schofield, J. E., Edwards, K. J., and Martínez Cortizas, A.: Industrial-era lead and mercury
938 contamination in southern Greenland implicates North American sources, Sci. Total
939 Environ., 613–614, 919–930, https://doi.org/10.1016/j.scitotenv.2017.09.041, 2018.

940 Pritchard, H., Arthern, R., Vaughan, D., and Edwards, L.: Extensive dynamic thinning on the
941 margins of the Greenland and Antarctic ice sheets, Nature, 461, 971–975,
942 https://doi.org/10.1038/nature08471, 2009.

943 Ramsey, C. B. and Lee, S.: Recent and Planned Developments of the Program OxCal,
944 Radiocarbon, 55, 720–730, https://doi.org/10.1017/S0033822200057878, 2013.

945 Reimer, P. J., Austin, W. E. N., Bard, E., Bayliss, A., Blackwell, P. G., Ramsey, C. B., Butzin,
946 M., Cheng, H., Edwards, R. L., Friedrich, M., Grootes, P. M., Guilderson, T. P., Hajdas, I.,
947 Heaton, T. J., Hogg, A. G., Hughen, K. A., Kromer, B., Manning, S. W., Muscheler, R.,
948 Palmer, J. G., Pearson, C., Plicht, J. van der, Reimer, R. W., Richards, D. A., Scott, E. M.,
949 Southon, J. R., Turney, C. S. M., Wacker, L., Adolphi, F., Büntgen, U., Capano, M., Fahrni,
950 S. M., Fogtmann-Schulz, A., Friedrich, R., Köhler, P., Kudsk, S., Miyake, F., Olsen, J.,
951 Reinig, F., Sakamoto, M., Sookdeo, A., and Talamo, S.: The IntCal20 Northern Hemisphere
952 Radiocarbon Age Calibration Curve (0–55 cal kBP), Radiocarbon, 62, 725–757,
953 https://doi.org/10.1017/RDC.2020.41, 2020.

954 Richter, A., Rysgaard, S., Dietrich, R., Mortensen, J., and Petersen, D.: Coastal tides in
955 West Greenland derived from tide gauge records, Ocean Dyn., 61, 39–49,
956 https://doi.org/10.1007/s10236-010-0341-z, 2011.

957 Saenko, O. A., Yang, D., and Myers, P. G.: Response of the North Atlantic dynamic sea
958 level and circulation to Greenland meltwater and climate change in an eddy-permitting ocean
959 model, Clim. Dyn., 49, 2895–2910, https://doi.org/10.1007/s00382-016-3495-7, 2017.

960 Shotyk, W., Goodsite, M. E., Roos-Barraclough, F., Frei, R., Heinemeier, J., Asmund, G.,
961 Lohse, C., and Hansen, T. S.: Anthropogenic contributions to atmospheric Hg, Pb and As
962 accumulation recorded by peat cores from southern Greenland and Denmark dated using
963 the 14C "bomb pulse curve," Geochim. Cosmochim. Acta, 67, 3991–4011,
964 https://doi.org/10.1016/S0016-7037(03)00409-5, 2003.

965 Spada, G. and Melini, D.: SELEN4; (SELEN version 4.0): a Fortran program for solving the
966 gravitationally and topographically self-consistent sea-level equation in glacial isostatic
967 adjustment modeling, Geosci. Model Dev., 12, 5055–5075, https://doi.org/10.5194/gmd-12-
968 5055-2019, 2019.

969 The IMBIE Team: Mass balance of the Greenland Ice Sheet from 1992 to 2018, Nature, 579,
970 233–239, https://doi.org/10.1038/s41586-019-1855-2, 2020.

971 Vogt, T.: Late-Quaternary Oscillations of Level in Southeast Greenland., Oslo: Dybwad
972 1933., 44 pp., 1933.

973 Wada, Y., Lo, M.-H., Yeh, P. J.-F., Reager, J. T., Famiglietti, J. S., Wu, R.-J., and Tseng, Y.-
974 H.: Fate of water pumped from underground and contributions to sea-level rise, Nat. Clim.
975 Change, 6, 777–780, https://doi.org/10.1038/nclimate3001, 2016.

976 Wangner, D. J., Sicre, M., Kjeldsen, K. K., Jaeger, J. M., Bjørk, A. A., Vermassen, F., Sha,
977 L., Kjær, K. H., Klein, V., and Andresen, C. S.: Sea Surface Temperature Variability on the
978 SE-Greenland Shelf (1796–2013 CE) and Its Influence on Thrym Glacier in Nørre

979 Skjoldungesund, Paleoceanogr. Paleoclimatology, 35,
980 https://doi.org/10.1029/2019PA003692, 2020.

981 Wood, K. R. and Overland, J. E.: Early 20th century Arctic warming in retrospect, Int. J.
982 Climatol., 30, 1269–1279, https://doi.org/10.1002/joc.1973, 2010.

983 Woodroffe, S. A. and Long, A. J.: Salt marshes as archives of recent relative sea-level
984 change in West Greenland, Quat. Sci. Rev., 28, 1750–1761, 2009.

985 Woodroffe, S. A. and Long, A. J.: Reconstructing recent relative sea-level changes in West
986 Greenland: local diatom-based transfer functions are superior to regional models, Quat. Int.,
987 221, 91–103, 2010.

988 Zheng, J.: Archives of total mercury reconstructed with ice and snow from Greenland and
989 the Canadian High Arctic, Sci. Total Environ., 509–510, 133–144,
990 https://doi.org/10.1016/j.scitotenv.2014.05.078, 2015.

991

992

993